ELSEVIER

Surface Science 437 (1999) 330–352

surface science

www.elsevier.nl/locate/susc

Image potential states on metal surfaces: binding energies and wave functions

E.V. Chulkov [a,*], V.M. Silkin [a,b], P.M. Echenique [a]

[a] *Departamento de Física de Materiales y Centro Mixto CSIC-UPV/EHU, Universidad del País Vasco/Euskal Herriko Unibertsitatea, Apdo. 1072, 20018 San Sebastian/Donostia, Spain*

[b] *Institute of Strength Physics and Materials Science, Russian Academy of Sciences, pr. Academicheskii 2/1, 634021 Tomsk, Russia*

Received 4 March 1999; accepted for publication 11 May 1999

Abstract

We present self-consistent pseudopotential calculations of both surface and image potential states on simple metal surfaces: Li(110), Na(110), Be(0001), Mg(0001), Al(100), and Al(111). The local density approximation (LDA) is used to describe the one-electron potential inside the film and in the surface region. In the vacuum space (at $z > z_{im}$) the LDA potential is replaced by the image potential. A one-dimensional potential proposed recently is constructed for 14 simple and noble metal surfaces. By using this model potential we study wave functions and binding energies of the image states and also image plane position trends for these metal surfaces. © 1999 Elsevier Science B.V. All rights reserved.

Keywords: Alkali metals; Alkaline earth metals; Aluminium; Copper; Density functional calculations; Semi-empirical models and model calculations; Silver; Surface electronic phenomena

1. Introduction

A metal surface generates electron states that do not exist in a bulk metal. These states can be classified into two groups according to their charge density localization relative to the surface atomic layer: intrinsic surface states and image potential states. The intrinsic surface states, predicted by Tamm [1] and Shockley [2], are localized mainly at the surface atomic layer. The image potential states are generated by a potential well formed by the Coulomb-like attractive image potential barrier $V(z) = -\frac{1}{4}(z - z_{im})$ and the repulsive surface barrier [3–9]. This potential well gives rise to the image potential states localized mostly in the vacuum region of metal surfaces (beyond the image plane position z_{im}) [3,4]. In a hydrogenic model these states form a Rydberg-like series with energies [3,4]

$$E_n = \frac{-0.85\ \text{eV}}{(n+a)^2}, \tag{1}$$

converging toward the vacuum level $E_V = 0$. The lifetime τ_n of these states scales asymptotically with the quantum number n $\tau_n \propto n^3$ [3,4]. In Eq. (1) a is a quantum defect that depends on the surface of interest. In particular, it depends on the width of the energy gap and its position relative to the vacuum level.

The binding energies of the image states have been extensively measured by inverse photoemission (IPE) [5,6,8–11], two-photon photoemission

* Corresponding author. Fax: +34-943-212236.
E-mail address: waptctce@sq.ehu.es (E.V. Chulkov)

0039-6028/99/$ – see front matter
PII: S0039-6028(99)00668-8

(2PPE) [12–14] and time-resolved two-photon photoemission (TR2PPE) [15–18] techniques. These measurements have provided highly accurate data of image states binding energies at surfaces of many noble and transition metals, such as Cu(100), Cu(111), Ag(100), Ag(111), Au(100), Au(111), Ni(100), Ni(111), Pd(111), Fe(110), Co(0001), Ru(0001). Information on the exchange splitting of such states has also been obtained [11,19–21]. Intrinsic line widths of image states associated with electron-hole pair excitations have been measured by means of 2PPE [14] and TR2PPE [16–18,22]. 2PPE measurements give a value of 5–25 fs for the lifetime of the first image state on many noble and transition metal surfaces [14]. The most recent TR2PPE measurements have given 40–50 fs for the first image state on Cu(100) and Ag(100) [17,23], 15–18 fs for Cu(111) [16,23], and 30 fs for Ag(111) [24]. Moreover, Höfer et al. [17] have measured the lifetime of the first six image states on Cu(100) using TR2PPE in combination with coherent excitation of several quantum states.

Many model and first-principles calculations have been performed to obtain binding energies and wave functions of image states [3,4,9,25–45]. In particular, it was shown that for surfaces like Cu(100) and Cu(111), on which the first image state is located in the middle and at the top of the s–p energy gap respectively, different parametrized models give the binding energies in quantitative agreement with experimental results [9,30,46], whereas wave functions of these states are reproduced only semi-quantitatively. First-principles calculations of the electronic structure of metal surfaces give an accurate description of wave functions and binding energies of both the surface and image states [25]. These evaluations with various degrees of sophistication have been performed for image states lying inside the energy gap, i.e. separated from bulk states, for Cu(100) [25], Ni(100) [39], Fe(110) [27], Au(100) [42], Ag(100) [43], Pd(100) [45], and Pd(111) [45]. Resonance image states that exist outside the energy gap and degenerate with bulk states have been computed as well. These calculations were performed within both the slab model (pseudopotential calculations) [38,40,41,45] and semi-infinite crystal model (the embedded method and the layer KKR method) [39,44,47] for Al(100) [38–40,45], Al(111) [40,41,45], Fe(110) [47], and Fe(100) [44].

Despite extensive measurements of image states on noble and transition metal surfaces, there is only one surface of simple metals on which the first image state has been studied experimentally, namely Al(111) [48–50]. Both IPE [48,49] and 2PPE [50] measurements give a binding energy of ~ -0.5 eV. Simple model calculations [33,34] and recent a first-principles evaluation [45] reproduce the experimental observation. At the same time a larger value $E_1 \simeq -0.9$ eV has been obtained in Refs. [28,36,41]. Finocchi et al. [41] argued that the origin of such large difference between theoretical [41] and experimental values is the low resolution of IPE. The single structure at -0.54 eV observed in IPE probably contains both the $n=1$ and $n=2$ image resonances. An interpretation of other IPE experiment [49] was based on a calculation by Papadia et al. [26] who obtained $E_1 = -0.47$ eV. A more accurate calculation performed recently by the same group gave $E_1 \simeq -1$ eV [28]. Bulovič et al. [50] have found an extremely weak feature in their 2PPE spectra around -0.45 eV and interpreted this feature as the first image state.

There are several calculations for the Al(100) surface [36–41,45]. As in the case of Al(111), these calculations give very different results lying in an energy interval 0.4–0.95 eV below the vacuum level. So, up to now, there has been no clear theoretical or experimental evidence as to what value of the first image state binding energy is the correct one. Apart from aluminium surfaces, theoretical calculations have only been performed for Na(110) [41] and for Li(110) [51]. On both these surfaces the binding energy was found to be $E_1 \simeq -0.7$ eV.

In contrast to many calculations of binding energies of image states, only a few evaluations of the lifetime of these states have been carried out [14,51–59]. Calculations performed within a self-energy formalism by Echenique and coworkers [52–54] have shown that the lifetime of image states crucially depends on the penetration of these states into the bulk and, therefore, an accurate description of the image states wave function is

needed. Deisz et al. [55], Gao and Lundqvist [56], and Osma et al. [58] have demonstrated the important role of final states, in particular the surface states, in the decay of image states. First-principles calculations of the image states lifetimes are limited by the complexity of a description of the screened Coulomb interaction for large systems [52–55]. Therefore, for practical calculations of the lifetime, a model that includes an accurate description of the binding energy and spatial behaviour of both the image and surface states is needed.

Recently, a model potential that has a constant value in the x, y plane and varies in the z direction was proposed by Chulkov and coworkers [51,57] to evaluate wave functions and binding energies of image states and also lifetimes of these image states. The key parameters of this potential reproduce experimental or first-principles calculation values of the width and position of the energy gap and energies E_0 and E_1 of the intrinsic or resonance surface state ($n=0$) and the first image state respectively. Preliminary calculation results for Li(110), for copper and silver surfaces, have been presented in Ref. [51]. We here apply this model to the simple metal surfaces of Na(110), Be(0001), Mg(0001), Al(100), and Al(111) and also to the (100) and (111) surfaces of gold and palladium. We also give an extended analysis of the model potential calculation results for lithium, copper and silver surfaces. A description of the potential is presented in Section 2. The results of the model potential calculations and discussion of binding energies and wave functions of image states and, also, of image plane positions for the simple and noble metal surfaces, are given in Section 3. The parameters of the potential for all surfaces of interest are given in Appendix A.

In this study we also present first-principles pseudopotential calculations of resonance image states on simple metal surfaces. We show that for all these surfaces the binding energy of the $n=1$ image state lies in an energy interval 0.7–0.9 eV below the vacuum level. We demonstrate that the Be(0001) surface is the best candidate among the simple metal surfaces to observe the first resonance image state experimentally. In contrast to the aluminium, magnesium, and sodium surfaces, it manifests a pronounced peak in the density of states corresponding to the first image state. The pseudopotential method is briefly described in Section 2, and in Section 3 we present the results of the pseudopotential calculation of simple metal surfaces. General discussion and conclusions are placed in Section 4.

2. Calculation methods

To calculate the electronic structure of simple metal surfaces we use a self-consistent pseudopotential method and a supercell technique. The norm-conserving non-local ion pseudopotential of lithium is generated according to Ref. [60], the norm-conserving ion pseudopotentials of Na, Be, Mg, and Al are constructed according to Refs. [61,62]. A local density approximation (LDA) is used for the exchange-correlation potential [63,64]. The calculations are carried out for 19–27-layer films. As the LDA does not reproduce the correct asymptotic behaviour of the image potential in the vacuum, the final iteration is carried out with the use of a modified potential that for $z<z_{\mathrm{im}}$ is the self-consistent LDA one and for $z>z_{\mathrm{im}}$ is given by Eq. (5) (see below). At this iteration the vacuum interval between consecutive films is chosen to be large enough ($\sim$20 interlayer spacings) to describe accurately the first image state wave function. For Li(110) this interval has been increased in order to describe also the second image state. The image plane position z_{im} is obtained as the centre of gravity of the charge density induced by a weak static electric field [51]. The values of z_{im}, obtained in this way, agree in general with those found in self-consistent calculations of linear response of a jellium to an external electric field [65] and to a test charge [66] and with those values obtained in calculations that take into account the non-local exchange-correlation contribution to form the correct asymptotic behaviour of the image potential [38,45,67]. At the same time, our z_{im} is always smaller than z_{im} obtained from the jellium model as a centre of gravity of the induced charge density [65]. This trend is caused by the effects of the crystal structure of a film. A similar trend was found by Serena et al. [68] for Li(110), by Heinrichsmeier et al. [45] for Al(100) and Al(111),

and also by White et al. [69] for Al(111). In the jellium model the dependence of z_{im} on the crystallographic face is determined by half an interlayer spacing $z_{im}=a_s/2+z_{im}^{jel}$, where z_{im}^{jel} is the image plane position defined relative to the jellium (geometrical) edge and a_s is the interlayer spacing. The factor $a_s/2$ gives artificially strong dependence of z_{im} on the crystallographic face. Because of this we compare our z_{im} with the jellium calculation results only for close-packed BCC(110), HCP(0001), and FCC(111) surfaces. The electronic self-energy calculations performed within the GW approximation [38,45,69] and the weighted-density approximation [67] place the image plane position closer to the surface atomic layer than our calculations do. This shift of z_{im} is dictated by the exchange correlation interaction of an electron being in an image state with remaining electrons of the system. The image plane position differences between our results and data of Refs. [38,65,67,69,70] do not influence significantly the binding energy of the first image state (this influence is practically negligible for the second and higher terms of the Rydberg series). For instance, for Li(110), a change in z_{im} of 0.6 a.u. brings a change of about 0.06 eV in E_1. For other simple metal surfaces, such as Be(0001), Al(100) and Al(111), the corresponding change in E_1 is of order of 0.10–0.15 eV. A similar slight dependence of the E_1 value on the image plane position was found by Nekovee and Inglesfield for Ni(100) [39].

The amplitude of image states is located relatively far from the surface [3,4] and, consequently, the effect of surface corrugation on these states is practically negligible [3,4,25]. This is the case for all surfaces studied in the present work, and, therefore, a one-dimensional model is applicable to these surfaces. One exceptional example of strong influence of the surface corrugation on image states, namely the Be($10\bar{1}0$) surface, has been studied [71]. Many one-dimensional potentials have been proposed to study binding energies and wave functions of image states [9,30–37]. As a rule these potentials are not smooth; they are continuous outside the crystal, but the first potential derivative is not a continuous function. These potentials have been constructed in order to calculate binding energies of image states for comparison with experimental results, and the image plane position was used as a fitting parameter of a model. Our potential and its first derivative are continuous everywhere in space. The energies E_0 and E_1 of the surface state and of the first image state respectively are the fitted parameters. We obtain z_{im} as a consequence of the model. For a description of the surface electronic structure we present a one-dimensional periodic-film model with large intervals between films. In this model the full screened potential has a constant value in the x, y plane and varies in the z direction as

$$V_1(z)=A_{10}+A_1\cos\left(\frac{2\pi}{a_s}z\right), \quad z<D \tag{2}$$

$$V_2(z)=-A_{20}+A_2\cos[\beta(z-D)], \quad D<z<z_1 \tag{3}$$

$$V_3(z)=A_3\exp[-\alpha(z-z_1)], \quad z_1<z<z_{im} \tag{4}$$

$$V_4(z)=\frac{\exp[-\lambda(z-z_{im})]-1}{4(z-z_{im})}, \quad z_{im}<z. \tag{5}$$

Here D is the half-width of the film, and the origin is taken at the middle plane of the film. The potential Eqs. (2)–(5) has ten parameters: A_{10}, A_1, A_{20}, A_2, β, A_3, α, z_1, λ, z_{im}; only four of them are independent. We choose A_{10}, A_1, A_2 and β as adjustable parameters. The other six parameters are determined from the requirement of continuity of the potential and its first derivative everywhere in space. The first term of the potential [Eq. (2)] describes the behaviour of the bulk potential that is terminated at the surface atomic layer. The parameters A_1 and A_{10} reproduce the width and position of the energy gap respectively. The solid–vacuum interface region is represented by Eqs. (3) and (4). The parameters A_2 and β of Eq. (3) reproduce experimental or first-principles calculation values E_0 and E_1 of the s–p surface state and the first image state respectively, at the $\bar{\Gamma}$ point. The intermediate point z_1 determined relative to the surface atomic layer is given by $z_1=5\pi/(4\beta)$, and $V_2(z_1)=-A_2/\sqrt{2}$. The position of image plane z_{im} is automatically obtained from the potential Eqs. (2)–(5) if the parameters A_1, A_{10}, A_2 and β reproduce the key features of the bulk and surface electronic structure. We illustrate schematically the model potential Eqs.

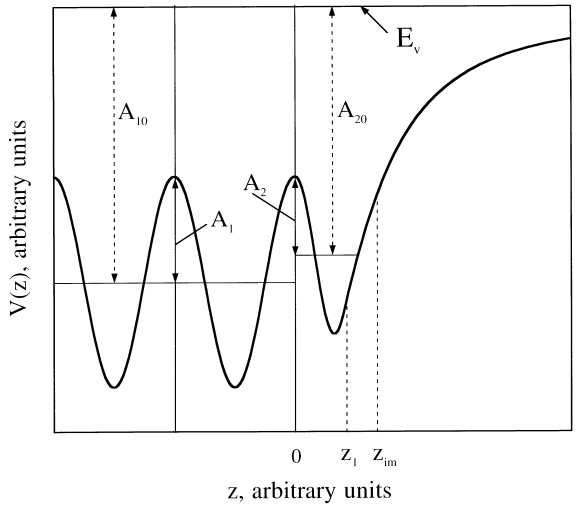

Fig. 1. Schematic plot of the model potential used. Vertical solid lines represent atomic layers positions.

(2)–(5) in Fig. 1 in the region where the solid–vacuum interface potential merges smoothly into an image-like Coulomb potential represented by Eq. (5). We also use an experimental or first-principles calculation work function value to fix the Fermi level position relative to the vacuum level. In fact, this parameter is not an adjustable; it may be obtained from band structure calculation with the potential Eqs. (2)–(5). In this case the difference between calculated and experimental values is of the order of 0.1 eV. However, for a more precise description of the electronic structure in the $E_V - E_F$ energy interval, we use the experimental value of work function. For all surfaces of interest, 500–700 atomic layer films with a 100–150 interlayer spacing vacuum interval between them have been used. Such a geometry allows us to resolve resonance surface states and resonance image states ($n=1, \ldots, 4$) with an accuracy better than 0.005 eV.

To obtain the binding energy of unoccupied resonance surface states unknown explicitly from an experiment for the Cu(100) and Pd(100) surfaces we have used a self-consistent linearized augmented-plane-wave (LAPW) film method [72,73]. The self-consistent calculations have been performed for nine-layer films of these metal surfaces. To find the width and position of the energy gaps unknown from experiments we calculate the bulk electronic structure of simple metals using the bulk pseudopotential version. The electronic structure calculation of bulk Cu, Ag and Pd is carried out with the use of the bulk version of the LAPW method.

3. Calculation results and discussion

3.1. Li(110)

We have performed self-consistent pseudopotential calculations of the surface electronic structure of Li(110) for a 27-layer film. Some characteristics of this structure are presented in Table 1.

As follows from the calculation, there are no occupied surface states on this surface. An unoccupied resonance surface state is obtained just below the wide energy gap at $\bar{\Gamma}$. The first and second image states are found in the energy gap just below the upper edge of the gap [51]. Our calculated work function $\phi = 3.35$ eV is in agreement with other calculation results [68,77,78] and the experimental value obtained for polycrystalline samples [76].

To fit the model potential parameters A_1 and A_{10} we use the lower and upper edge positions of the energy gap found in our bulk calculation. The lower edge position is in excellent agreement with the results of other calculations performed within both the LDA [74,75,80] and the quasi-particle approximation [75], whereas there is some disagreement between the LDA and the quasi-particle evaluations for the upper edge. The LDA calculations [51,74,75] give for this position a value that is closer to the vacuum level by ~ 0.5 eV than the quasi-particle theory does [75]. This shift can influence the first image state. Our pseudopotential calculation gives $E_1 = -0.73$ eV relative to E_V. It is located at -0.62 eV relative to the LDA upper edge of the gap and at -0.02 eV relative to the quasi-particle upper edge position. How does this proximity of an image state to the upper edge have an influence on its characteristics? As follows from IPE and 2PPE measurements [6,8,14,81,82], the $n=1$ state is located in the middle of the gap on

Table 1
Some characteristics of the Li(110) surface. The lower edge E_{edge}^{lower}, the upper edge E_{edge}^{upper} of the energy gap and surface state energy E_0 are expressed relative to the Fermi level E_F. Image states energies E_n are given relative to the vacuum level $E_V=0$. All energies and work function ϕ are in electron-volts. Penetration values p_n are given in percent. The symbol * marks resonance state. The image plane position z_{im} is given in a.u. relative to the surface atomic layer

Characteristics	Experiment	Theory	Model potential
E_{edge}^{lower} (N_1')	–	0.25[a]; 0.21[b]; 0.27[c]; 0.25[c]	0.25
E_{edge}^{upper} (N_1)	–	3.24[a]; 3.10[b,c]; 2. 64[c]	3.24
E_0^*	–	0.18[a]	0.18
E_1	−0.73[d]	−0.73[a]	−0.73
E_2	−0.197[d]	−0.22[a]	−0.217
E_3^*	−0.090[d]	–	−0.100±0.002
E_4^*	−0.051[d]	–	−0.055±0.002
p_1	–	15.05[a]	15.27
p_2	–	5.78[a]	5.89
ϕ	2.93[e]	3.35[a]; 3.45[f]; 3.55[g];3.63[h]; 3.33[i]	3.35
z_{im}	–	3.63[a]; 3.2[h]; 3.74[j]; 2.93[k]; 3.08[l]	3.21

[a] Present calculation.
[b] Ref. [74].
[c] Ref. [75].
[d] This value is obtained from the conventional Eq. (1), where $a=\sqrt{0.85/E_1}-1$. E_1 is the experimental or first-principles calculation energy value of the $n=1$ image state.
[e] Ref. [76].
[f] Ref. [77].
[g] Ref. [78].
[h] Ref. [68].
[i] Ref. [79].
[j] Ref. [65].
[k] Ref. [67].
[l] Ref. [70].

the Cu(100), Ag(100), Pd(111) surfaces and energy of this state is ~ -0.55 eV relative to E_V. A different situation is observed for Cu(111), Ag(111), and Au(111), where, as for Li(110), the upper edge of the energy gap is just below E_V [3,4,6,14,81]. On Ag(111) and Cu(111) the $n=1$ state is located ~ 0.1 eV below the upper edge, and its energy is -0.77 eV for Ag(111) [14,81] and -0.82 eV for Cu(111) [14,16]. On Au(111) this state with the energy of -0.80 eV degenerates with bulk states, i.e. it is above the upper edge. Following this analogy one can expect that the binding energy of the first image state on Li(110)

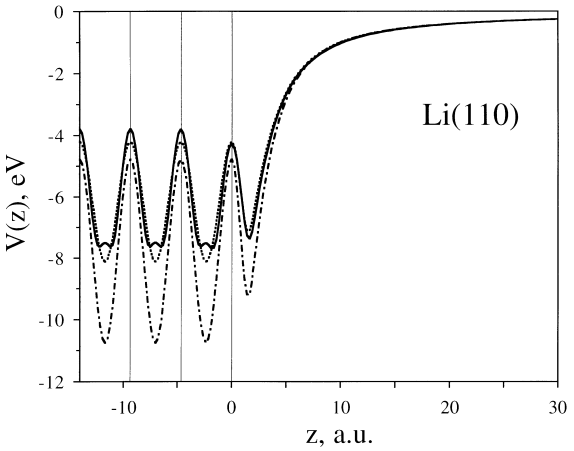

Fig. 2. The local part of the full screened pseudopotential averaged in the plane parallel to the surface (solid line), the model potential, reproducing correctly the energy gap width and position (dot–dashed line), and the model potential, reproducing the results of the calculation performed with use of the local part of the screened pseudopotential (dotted line) for Li(110). $z=0$ corresponds to the surface atomic layer position. Vertical solid lines represent atomic layers positions.

may be increased from -0.73 eV in the LDA calculation up to -0.80 eV in the quasi-particle calculation. This 10% increase of the binding energy does not change significantly the properties of the $n=1$ state obtained in the present calculation. At the same time, lowering of the position of the upper energy gap edge can change the properties of the second image state. This state will degenerate with bulk states. As we concentrate mainly on the first image state (this state is used to fit the parameters A_2 and β), we utilize here the surface electronic structure data from the LDA calculation.

In Fig. 2 we compare the one-dimensional model potential calculated for Li(110) and the local part of the full screened non-local self-consistent pseudopotential averaged in a plane parallel to the surface. The discrepancy between these two curves is explained by the absence of the non-local contribution, which is a large one for lithium [60]. The use of the averaged local contribution only modifies the energy gap. It gives different positions of the edges of the energy gap and different binding energies of the image states [51]. The model potential constructed for the modified energy gap (for

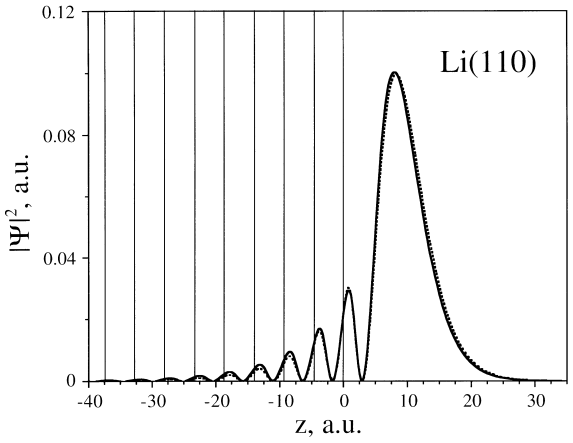

Fig. 3. The probability amplitude of the first image state of the Li(110) surface obtained from the model potential (solid line) and from the full pseudopotential (dotted line) calculation. Vertical solid lines represent atomic layers positions.

that we have changed only the parameters A_{10} and A_1) is also shown (dashed line) in Fig. 2. As follows from the figure, good agreement is observed between the local part of the pseudopotential and the modified model potential. Both of them give practically the same binding energy of the $n=1$ state: $E_1 \approx -0.52$ eV. This result confirms the importance of the energy gap parameters for a description of image states found previously [3–9,14,29–31].

In order to test the quality of the image states wave functions, obtained with the use of the model potential, we compare in Fig. 3 the probability amplitudes of the first image state found in the non-local pseudopotential calculation as well as in that of the model calculation. One can see in Fig. 3 that the difference between these two curves is very small, especially in the vicinity of the surface atomic layer. Very similar results are obtained for the second image state and for the surface resonance. These results show that the model potential Eqs. (2)–(5) describes with high accuracy both the binding energies and wave functions of the image states as well as of the surface state.

The finite lifetime value of image states is due to the coupling to bulk and surface states. The decay into unoccupied states is accompanied by the creation of electron–hole pairs. A measure of this coupling is the charge fraction (penetration) of the image state inside the crystal. In Table 1 we give the calculated penetration values p_n for the $n=1, 2$ states (we assume that the crystal edge is located at half an interlayer spacing from the last atomic layer). p_n is defined as a fraction of the nth image state in the bulk. The evaluated penetration $p_1=15.27\%$ of the $n=1$ state is significantly closer to that obtained for Cu(111) and Ag(111) than to that found for Cu(100) and Ag(100) [51]. The image states binding energies $E_2=0.217$ eV, $E_3=0.100$ eV, and $E_4=0.055$ eV found in the model potential calculation are in agreement with the E_n values obtained from Eq. (1). The inaccuracy of the binding energies of the resonance surface states obtained from the one-dimensional model potential Schrödinger equation is explained by the use of the finite film thickness. The image plane position, $z_{\mathrm{im}}=3.21$ a.u., agrees well with the pseudopotential calculation result [68] and evaluation data of Appelbaum and Hamann [70] and Ossicini et al. [67].

3.2. Na(110)

In Table 2 we show some experimental and calculation data characterizing the electronic structure of Na(110). The projection of the bulk band structure of Na onto the (110) surface is similar to that of lithium. The lower edge position of the energy gap obtained from the pseudopotential evaluation of bulk band structure agrees well with other LDA [74,75] calculations and quasi-particle [75] results. So, we use $E(N_1)=0.68$ eV together with our energy value of the upper edge to fit the parameters A_1 and A_{10}. As in the case of Li(110), a broad surface resonance state with energy of 0.45 eV relative to E_{F} has been found at $\bar{\Gamma}$ just below the energy gap in our slab pseudopotential calculation. But, in contrast to the Li(110) surface, all image states on Na(110) are the resonance ones. In the calculated vacuum density of states there appear peaks that correspond to the $n=$ 2, 3, … image states, whereas the $n=1$ image state peak does not appear. Therefore, we determine the binding energy of the first image resonance as the mean energy of the film electron states having one node just around the crystal edge or in the vacuum and weighted for each of these states by

Table 2
The Na(110) surface (designations and units correspond to those in Table 1)

Characteristics	Experiment	Theory	Model potential
E_{edge}^{lower} (N_1')	–	0.73[a]; 0.82[b]; 0.67[b]; 0.68[c]	0.68
E_{edge}^{upper} (N_1)	–	1.11[a]; 1.35[c]	1.35
E_0^*	–	0.45[c]; 0.69[d]	0.60
E_1^*	−0.77[e]	−0.77[c]; −0.71[d]	−0.77±0.02
E_2^*	−0.202[e]	−0.20[d]	−0.206±0.002
E_3^*	−0.091[e]	–	−0.094±0.002
E_4^*	−0.052[e]	–	−0.052±0.002
ϕ	2.9[f]; 2.75[g]	3.0[c]; 3.10[h,i]; 2.94[j]	2.9
z_{im}	–	4.10[c]; 4.18[k]; 3.33[l]; 3.48[m]	4.0

[a] Ref. [74].
[b] Ref. [75].
[c] Present calculation.
[d] Ref. [41].
[e] This value is obtained from the conventional Eq. (1), where $a=\sqrt{0.85/E_1}-1$. E_1 is the experimental or first-principles calculation energy value of the $n=1$ image state.
[f] Ref. [83].
[g] Ref. [84].
[h] Ref. [78].
[i] Ref. [85].
[j] Ref. [79].
[k] Ref. [65].
[l] Ref. [67].
[m] Ref. [70].

the integration of the probability amplitude in the vacuum region. The binding energy E_1, so calculated, is −0.77 eV, which agrees with the $E_1=-0.71$ eV obtained by Finocchi et al. [41] with the use of a model pseudopotential [86]. The parameters A_2 and β are found by reproducing reasonably the calculated broad resonance surface state energy and the first image state energy. Our model potential gives $E_2=-0.206$ eV in good agreement with that found in Ref. [41]. Excellent agreement is observed between the one-dimensional model potential Schrödinger equation eigenvalues and solutions of Eq. (1) for E_2, E_3, and E_4. As for the work function, our pseudopotential calculation gives $\phi=3.0$ eV, which agrees well with both the experimental data [84] and the calculation result [78]. The image plane position values 4.1 a.u. and 4.0 a.u., obtained from the pseudopotential and model potential evaluations respectively, are close to that found in the jellium model by Lang and Kohn [65]. However, some disagreement is observed with the calculations of Appelbaum and Hamann [70] and Ossicini et al. [67]. The reason for this disagreement in the case of the pseudopotential evaluation is, in fact, the use of the linear response to a test charge, when z_{im} is determined as a centre of gravity of the induced charge density. A more accurate treatment of the exchange correlation interaction may decrease z_{im} [38,69] to better agreement with the calculations [67,70].

3.3. Be(0001)

In contrast to the extensive study of the occupied electronic structure [87–91], to the best of our knowledge there are two experimental studies of the unoccupied electronic structure of Be(0001) [92,93]. Bruhwiller and coworkers [92,93] using the IPE technique observed a large peak just below E_V. They ascribed this feature to the image potential, but did not extract precise information from the peak to determine the binding energies of image states. The results obtained in the slab pseudopotential calculation are presented in Fig. 4 and in Table 3. As one can see in Fig. 4, the calculation gives well-known occupied surface states at $\bar{\Gamma}$, $\bar{M}$, and $\bar{K}$ [87–90]. Resonance image

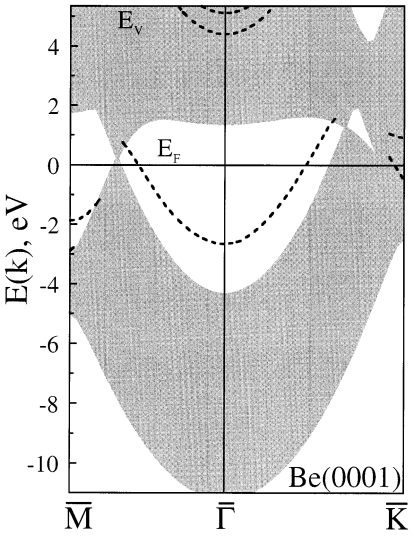

Fig. 4. Calculated surface electronic structure of Be(0001): the projected band structure of bulk Be and the surface and image states (dashed lines).

Table 3
The Be(0001) surface (designations and units correspond to those in Table 1)

Characteristics	Experiment	Theory	Model potential
E_{edge}^{lower} (Γ_{3+})	−4.8[a]	−4.34[b]; −4.3[c]	−4.8
E_{edge}^{upper} (Γ_{4-})	–	1.40[b]; 1.2[c]	1.4
E_0	−2.8[d]	−2.6[e]; −2.8[f]	−2.8
E_1^*	−0.95[g]	−0.95[b]	−0.95±0.01
E_2^*	−0.224[g]	–	−0.24±0.01
E_3^*	−0.098[g]	–	−0.096±0.002
E_4^*	−0.055[g]	–	−0.058±0.002
ϕ	5.1[h]	5.35[b]; 5.54[f]	5.35
z_{im}	–	2.75[b]; 3.31[i]; 2.57[j]; 2.72[k]	2.21

[a] Ref. [94].
[b] Present calculation.
[c] Ref. [74].
[d] Refs. [87,88].
[e] Ref. [89].
[f] Ref. [90].
[g] This value is obtained from the conventional Eq. (1), where $a=\sqrt{0.85/E_1}-1$. E_1 is the experimental or first-principles calculation energy value of the $n=1$ image state.
[h] Ref. [95].
[i] Ref. [65].
[j] Ref. [67].
[k] Ref. [70].

states with $n=1, 2$ are shown in the upper part of Fig. 4. The energies of these states are $E_1=-0.95$ eV and $E_2=-0.24$ eV. As in the case of Na(110), the E_1 and E_2 energies are determined by weighting the film electron states according to the fraction of the states in the vacuum region and to the position of the wave function node of these states relative to the crystal edge. The calculated work function value $\phi=5.35$ eV agrees reasonably well with the experimental one obtained for polycrystalline samples [95] and with the evaluation result [90]. In contrast to Na(110), the image plane position obtained for Be(0001) is in good agreement with that found in Refs. [67,70] for the charge density parameter r_s corresponding to bulk Be.

We fit the model potential parameters A_1 and A_{10} to the experimental value [94] of the lower edge of the gap and to our bulk calculation result for the upper edge. The parameters A_2 and β reproduce the experimental surface state energy at $\bar{\Gamma}$ [87,88] and the calculated value $E_1=-0.95$ eV. In Table 3 we show the binding energies of the $n=2, 3, 4$ image states and the image plane position obtained with the model potential; good agreement is observed between the one-dimensional model potential Schrödinger equation eigenvalues and solutions of Eq. (1).

In Fig. 5 the vacuum density of states evaluated with the model potential is shown for energies just below E_V. This DOS has been obtained by integration of the local density of states DOS(E, z) over the vacuum region. As can be seen in Fig. 5, there is a clear peak of the first image state at −0.95 eV in the DOS curve. Two other peaks correspond to the second and third image states. It is interesting to note that the clear peak of the first image state is also observed in the DOS curve that was obtained from a calculation with the local part of the full screened non-local pseudopotential averaged in a plane parallel to the surface. This remarkable feature differs drastically for the Be(0001) surface from other non-transition-metal surfaces. In particular, for Na(110), Mg(0001), Al(100), and Al(111) we could not obtain a clear DOS peak for the first image state. The only way to determine the $n=1$ state binding energy on these surfaces is weighting the film electron states by taking into account a node position of the wave functions. This difference may be qualitatively

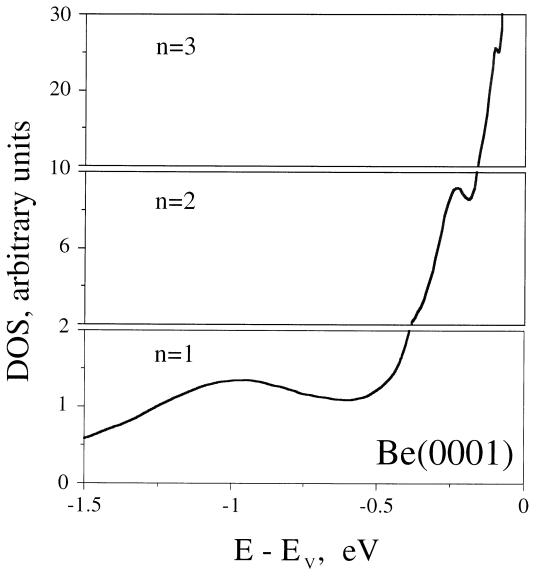

Fig. 5. Calculated vacuum density of states for Be(0001). The peaks corresponding to the $n=1, 2, 3$ image states are shown.

understood as a consequence of the higher electron reflectivity of the Be crystal, compared with other simple metals, that originates from the wide energy gap at the $\bar{\Gamma}$ point. The existence of a clear peak in the DOS of Be(0001) assumes that it might be much easier to observe experimentally the first image state on this surface than on both the (111) and (100) surfaces of aluminium.

3.4. Mg(0001)

The projected bulk band structure of magnesium onto the (0001) surface has a narrow energy gap with a width that was found experimentally to be of 0.7 eV at $\bar{\Gamma}$ [96], and LDA calculations give a width around 0.35 eV (see Table 4.). The present pseudopotential calculation of the surface electronic structure reproduces the LDA data published previously [89,99] and gives an energy of -0.78 eV for the first image state. The image plane position obtained, $z_{im}=3.66$ a.u., is in reasonable agreement with the results of Appelbaum and Hamann [70] and Lang and Kohn [65], whereas the weighted density approximation calculation [67] places z_{im} closer to the surface atomic layer by 0.5 a.u.

To fit the parameters A_1 and A_{10} we use the positions of the energy gap edges found in angle-resolved photoemission measurements [96]. The parameters A_2 and β are fitted to reproduce the experimental value of the surface state binding energy within the experimental error and the pseudopotential evaluation binding energy of the first image state. The image plane position, $z_{im}=3.46$ a.u., obtained from the model potential calculation agrees with all available theoretical results.

Table 4
The Mg(0001) surface (designations and units correspond to those in Table 1)

Characteristics	Experiment	Theory	Model potential
E_{edge}^{lower} (Γ_{3+})	-1.7 ± 0.1[a]	-1.53[b]; -1.58[c]	-1.7
E_{edge}^{upper} (Γ_{4-})	-0.9 ± 0.1[a]; -1.0[d]	-1.11[b]; -1.28[c]	-1.0
E_0	-1.6 ± 0.1a; -1.7[e]	-1.56[f,g]	-1.5
E_1^*	-0.78[h]	-0.78[c]	-0.78 ± 0.04
E_2^*	-0.203[h]	–	-0.21 ± 0.01
E_3^*	-0.092[h]	–	-0.100 ± 0.004
E_4^*	-0.052[h]	–	-0.056 ± 0.004
ϕ	3.66[i]	3.7[f]; 4.05[i]; 3.86[j]	3.66
z_{im}	–	3.66[c]; 3.96[k]; 3.18[l]; 3.33[m]	3.46

[a] Ref. [96].
[b] Ref. [74].
[c] Present calculation.
[d] Ref. [97].
[e] Ref. [98].
[f] Ref. [89].
[g] Ref. [99].
[h] This value is obtained from the conventional Eq. (1), where $a=\sqrt{0.85/E_1}-1$. E_1 is the experimental or first-principles calculation energy value of the $n=1$ image state.
[i] Ref. [78].
[j] Ref. [79].
[k] Ref. [65].
[l] Ref. [67].
[m] Ref. [70].

3.5. Al(100) and Al(111)

The Al(100) surface is one of the most studied theoretically among simple metal surfaces. However, in contrast to the case of surface states detected experimentally at different symmetry points [100–102] and obtained theoretically [38,40,103–109], no measurements of image states have been performed for Al(100). Theoretical calculations of the first image state energy give values lying in a wide energy interval: from -1.0 eV to -0.4 eV (see Table 5). On the one hand, this large spread in energy may be attributed to the resonance character of the image state, and on the other hand to different positions of the image plane used in the calculations. As we have shown for Li(110), the z_{im} value does not influence seriously the binding energy of the image states. The same occurs for Be(0001) and aluminium surfaces. So, one can expect that the real origin of the large spread in binding energy values is the resonance nature of the image state, i.e. theoretical results may depend on the way of weighting resonance states. Our slab pseudopotential calculation describes very well the surface electronic structure of Al(100). In particular, it gives a binding energy of -2.76 eV for the surface state at $\bar{\Gamma}$ that is in excellent agreement with photoemission measurements [100–102]. It gives a first image state binding energy of $E_1=-0.88$ eV, which agrees well with the results by Finocchi et al. [41], Jurczyszyn and

Table 5
The Al(100) surface (designations and units correspond to those in Table 1)

Characteristics	Experiment	Theory	Model potential
E_{edge}^{lower} ($X_{4'}$)	-2.83[a]	-2.86[b]; -2.96[c]; -2.99[d]	-2.83
E_{edge}^{upper} (X_1)	-1.15[a]	-1.79[b]; -1.64[c,d]	-1.15
E_0	-2.75[a,e]; -2.8[f]	-2.76[d]; -2.73[g]; -2.9[h]; -2.92[i]; -2.6[j]; -2.65[k]; -2.81[l]; -2.67[m]; -2.71[n]	-2.6
E_1^*	-0.88[o]	-0.88[d]; -0.4[n,t]; -0.95[p]; -0.65[q]; -0.59[r]; -0.8[s]	-0.88
E_2^*	-0.216[o]	-0.18[n]; -0.25[p]; -0.16[q]; -0.17[r]	-0.23 ± 0.01
E_3^*	-0.096[o]	-0.074[r]	-0.10 ± 0.01
E_4^*	-0.054[o]	–	-0.056 ± 0.003
ϕ	4.41[u]; 4.2[v]	4.49[g]; 4.7d,h; 4.54[k]; 4.67[l]; 4.41[m]; 4.82[n]; 4.63[q]; 4.59[t]; 4.2[p,w]; 4.27[x]; 4.5[y,z]	4.4
z_{im}	–	3.15[d]; 3.45[r]; 2.44[t]; 3.22[x]; 2.95[aa]; 3.0[ab]	3.44

[a] Ref. [100].
[b] Ref. [41].
[c] Ref. [110].
[d] Present calculation.
[e] Refs. [101,102].
[f] Ref. [111]
[g] Ref. [103].
[h] Ref. [104].
[i] Ref. [105].
[j] Ref. [106].
[k] Ref. [107].
[l] Ref. [108].
[m] Ref. [109].
[n] Ref. [38].
[o] This value is obtained from the conventional Eq. (1), where $a=\sqrt{0.85/E_1}-1$. E_1 is the experimental or first-principles calculation energy value of the $n=1$ image state.
[p] Ref. [74].
[q] Ref. [39].
[r] Ref. [37].
[s] Ref. [36].
[t] Ref. [45].
[u] Ref. [112].
[v] Ref. [113].
[w] Ref. [78].
[x] Ref. [68].
[y] Ref. [114].
[z] Ref. [115].
[aa] Ref. [116].
[ab] Ref. [117].

Stęślicka [36], and Nekovee and Inglesfield [39]. A larger difference is observed with the value of E_1 obtained by Eguiluz and coworkers [38,45]. In part, (~ 0.15 eV) this discrepancy may be related to the different z_{im} values found in the present work and in Ref. [38]. In their pseudopotential calculation of image states Eguiluz and coworkers [38,45] used $z_{im}=2.62$ a.u. resulting from the electronic self-energy evaluation of the jellium slab [38]. Decreasing z_{im} by 0.5 a.u. we find $E_1=-0.72$ eV, which is still significantly larger than that obtained in Ref. [38]. The reason for the remaining part of this discrepancy is still unclear to us. To verify our result for E_1 we performed the calculations for 27- and 301-layer films with the local part of the screened pseudopotential averaged in the x, y plane. For the 27-layer film this potential gives practically the same result as the three-dimensional non-local pseudopotential. A very similar value is obtained from the evaluation of a 301-layer film. The calculated work function is fairly close to the experimental value of 4.4 eV and agrees with other calculation results. Our value of $z_{im}=3.15$ a.u. is in reasonable agreement with the calculations that take into account the crystal structure of the Al(100) surface [37,68,116,117].

To determine the model potential parameters A_1 and A_{10} we utilize the experimentally found [100] positions of the lower and upper edges of the energy gap. The parameters A_2 and β are fitted to reproduce the experimental value of the binding energy of the surface state [100] within the experimental error and the pseudopotential calculation value $E_1=-0.88$ eV of the first image state. Our results for binding energies of the excited image states are in agreement with those found from Eq. (1) with $E_1=-0.88$ eV. Some disagreement is observed with the calculations [37–39] for the second image state, whereas our value of E_2 is very close to that obtained in Ref. [41]. The image plane position, $z_{im}=3.44$ a.u., found with the model potential agrees well with the value of z_{im} calculated by Lang and Kohn [65] and Radny [37].

In contrast to other simple metal surfaces, three measurements have been performed to determine the binding energy of the first image state on the Al(111) surface [48–50]. All of them give $E_1\approx -0.5$ eV below the vacuum level, whereas theoretical calculations lead to energies lying in a wide interval from -0.40 eV to -1.0 eV (see

Table 6
The Al(111) surface (designations and units correspond to those in Table 1)

Characteristics	Experiment	Theory	Model potential
E_{edge}^{lower} ($L_{2'}$)	–	−4.71[a]; −4.62[b]; −4.65[c]	−4.65
E_{edge}^{upper} (L_1)	–	−4.36[a]; −4.41[b]; −4.40[c]	−4.40
E_0	−4.56[d]	−4.53[c]; −4.69[e]; −4.68[f]; −4.6[g]	−4.54
E_1^*	−0.54[h]; −0.49[i]; −0.46[j]	−0.79[c]; −0.86[k]; −0.62[l]; −0.45[m]; −1.0[n]; −0.5[o]; −0.4[p]	−0.79
E_2^*	−0.205[q]	−0.24[k]; −0.16l,m	−0.22 ±0.01
E_3^*	−0.092[q]	−0.054[l]	−0.100 ±0.004
E_4^*	−0.052[q]	–	−0.055 ±0.004
ϕ	4.24[r]; 4.26[s]	4.40[c]; 4.49[e]; 4.28[f]; 4.19[g]; 4.18[k,t]; 4.82[p]; 4.05[u]; 4.25[v]	4.24
z_{im}	–	3.24[c]; 3.74[l]; 2 6[p,ab]; 3 3[t]; 3.78[w,x]; 3.03[y]; 3.18[z]; 2.91[aa]; 3.14[ac]; 3.0[ad]	3.49

[a] Ref. [74].
[b] Ref. [110].
[c] Present calculation.
[d] Ref. [118].
[e] Ref. [119].
[f] Ref. [120].
[g] Ref. [109].
[h] Ref. [48].
[i] Ref. [49].
[j] Ref. [50].
[k] Ref. [41].
[l] Ref. [37].
[m] Ref. [34].
[n] Ref. [28].
[o] Ref. [33].
[p] Ref. [45].
[q] This value is obtained from the conventional Eq. (1), where $a=\sqrt{0.85/E_1}-1$. E_1 is the experimental or first-principles calculation energy value of the $n=1$ image state.
[r] Ref. [112].
[s] Ref. [113].
[t] Ref. [68].
[u] Ref. [78].
[v] Ref. [114].
[w] Ref. [121].
[x] Ref. [65].
[y] Ref. [67].
[z] Ref. [70].
[aa] Ref. [38].
[ab] Ref. [69].
[ac] Ref. [122].
[ad] Ref. [66].

Table 6). Simplified models [33,34] and the first-principles calculation [45] give $E_1 \approx -0.5$ eV, whereas in the calculations [28,41] a value of $E_1 \approx -0.9$ eV has been obtained. Our self-consistent pseudopotential calculation gives the surface state energy at $\bar{\Gamma}$ in excellent agreement with both experimental values [118] and other calculation values [109,119,120], whereas the first image state energy $E_1 = -0.79$ eV agrees only qualitatively with available experimental data. Good agreement is observed with the calculations by Finocchi et al. [41] and by Fondén et al. [28]. The discrepancy with the evaluation by Jurczyszyn and Stęślicka may be attributed partly to the small value of $z_{im} = 2.2$ a.u. used in Ref. [34]. This value of z_{im} coincides with the jellium edge position of Al(111). Some part of the discrepancy with $E_1 = -0.4$ eV, found in Ref. [45], may also be attributed to the smaller $z_{im} = 2.6$ a.u. utilized by Heinrichsmeier et al. [45]. As was mentioned in Section 1, the large difference between the calculated values of $E_1 = -0.8$ to -1.0 eV and that measured by Heskett et al. [48] of $E_1 = -0.54$ eV may be explained by the relatively low resolution of the IPE spectroscopy technique. The discrepancy with other IPE experiments [49] may be attributed to an interpretation of the IPE data based on preliminary calculation results by Papadia et al. [26]. New calculations carried out by the same group gave $E_1 \approx -1$ eV [28]. At the same time Bulovič et al. [50] have obtained $E_1 \approx -0.45$ eV based on an extremely weak feature of the 2PPE spectra. So, both experimental and theoretical investigations of the image state on Al(111) show a very weak character of the resonance image state on this surface and illustrate problems arising from this character in the study of this state. The image plane position we obtain is in reasonable agreement with both the lattice and the jellium model evaluation results. The maximum discrepancy is observed with the electronic self-energy calculation by White et al. [69] and Heinrichsmeier et al. [45], and with the jellium evaluation by Lang and Kohn [65] of a response of a metal surface to an external electric field. The self-energy calculations place z_{im} closer to the surface atomic layer by ~ 0.6 a.u. than our evaluation does, whereas the linear response calculation shifts z_{im} outwards by ~ 0.6 a.u. [65].

The model potential parameters A_1 and A_{10} are fitted to our calculated position of the lower and

upper edges of the energy gap. A_2 and β reproduce our pseudopotential calculation binding energies of both the surface state and the first image state. Some results obtained with this potential are listed in Table 6 and, as can be seen, our E_2 value agrees well with that found by Finocchi et al. [41] but only semi-quantitatively with data from Refs. [34,37]. The image plane position found with the model potential lies between the pseudopotential calculation value and that obtained by Lang and Kohn [65] and Schreier and Rebentrost [121] from the jellium model.

3.6. Cu(100) and Cu(111)

Cu(100) is one of the most studied of metal surfaces. Numerous calculations and measurements of the electronic structure have been performed for this surface (e.g. see Refs. [10,25,123–125]). High precision measurements of the binding energies of the $n=1, 2$ image states have been done by 2PPE [14,126]. Cu(100) is the only surface for which very accurate values of the image states lifetime have been obtained experimentally for $n=1, 2, \ldots, 6$ [17]. Therefore, one can consider Cu(100) as one of the best candidates to verify any model pretending to describe and predict characteristics of the image potential states. In Table 7 we show a list of experimentally and theoretically determined electronic properties of Cu(100). The fourth column of Table 7 shows data $E(X_{4'})$, $E(X_1)$, E_0, E_1 used to fit the model potential parameters and energies E_2, E_3, E_4 obtained with this potential. Of the excited image states only E_2 was measured by 2PPE [126]. Our value $E_2=-0.18$ eV is in excellent agreement with this result. In Table 7 we compare the binding energies for the $n=2, 3, 4$ states obtained by direct solution of the Schrödinger equation using the model potential Eqs. (2)–(5) with those obtained from Eq. (1). The difference between these values does not exceed 6%.

Fig. 6 shows the probability amplitude of the $n=1, 2, ,3, 4$ image states obtained with the use of the model potential and compares the probability amplitude of the most sensitive to the surface potential corrugation first image state found in the first-principles (FLAPW) calculation [25] with that obtained from the present evaluation. Excellent agreement between these functions emphasizes, on the one hand, the small role of the surface corrugation in the formation of image potential states on Cu(100). On the other hand, this agreement testifies to the very good quality of the wave functions generated with the model potential Eqs. (2)–(5). The penetration $p_1=5\%$ agrees well with the FLAPW and wave function matching technique results [25].

In Table 7 we compare our image plane position value with those obtained with the use of different approaches [9,30,31,116,131]. Smith et al. [131]

Table 7
The Cu(100) surface (designations and units correspond to those in Table 1)

Characteristics	Experiment	Theory	Model potential
E_{edge}^{lower} ($X_{4'}$)	1.8[a]	1.75[b]; 1.6[c]	1.6
E_{edge}^{upper} (X_1)	7.9 ± 0.2[d]	6.9[b]; 7.7[c]	7.7
E_0^*	1.4[a]; 0.8[e]; 1.15[f]; 1.1[g]	1.0[c]; 0.5[e]; 0.2[h]	1.0
E_1	−0.5[a]; −0.57[i]; −0.6[j,k]	−0.62[e,l]; −0.52[h]	−0.57
E_2	−0.18[i]; −0.17[m]	−0.19[e]; − 0.18[l]	−0.18
E_3	−0.082[m]	−0.09[e]	−0.083
E_4	−0.048[m]	–	−0.051
p_1	–	3.4[n]	5.17
p_2	–	–	0.92
p_3	–	–	0.30
p_4	–	–	0.13
ϕ	4.62[n]	4.91[o]; 4.94[p]	4.62
z_{im}	–	1.01[h]; 2.48[l]; 2.18[q]; 2.33[q]; 2.40[r]; 1.93[s]	2.27

[a] Ref. [10].
[b] Ref. [74].
[c] Present LAPW calculation.
[d] Ref. [127].
[e] Ref. [25].
[f] Ref. [125].
[g] Ref. [128].
[h] Ref. [31].
[i] Ref. [126].
[j] Ref. [129].
[k] Ref. [130].
[l] Ref. [30].
[m] This value is obtained from the conventional Eq. (1), where $a=\sqrt{0.85/E_1}-1$. E_1 is the experimental or first-principles calculation energy value of the $n=1$ image state.
[n] Ref. [14].
[o] Ref. [123].
[p] Ref. [124].
[q] Ref. [131].
[r] Ref. [116].
[s] Ref. [9].

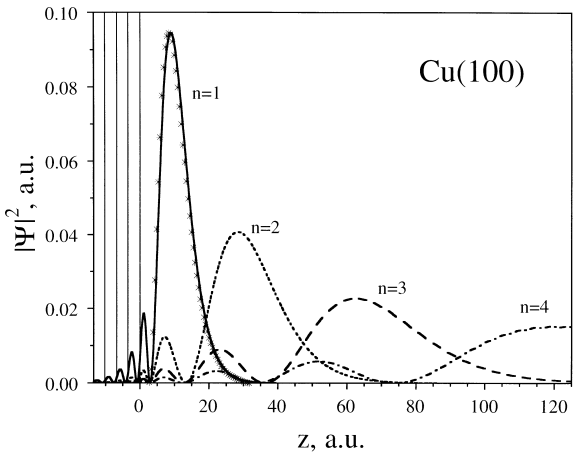

Fig. 6. The probability amplitude of the $n=1$, 2, 3, and 4 image states obtained from the model potential calculation are shown for the Cu(100) surface. Vertical solid lines represent atomic layers positions. $z=0$ corresponds to the surface atomic layer position. Asterisks represent the probability amplitude of the $n=1$ image state for Cu(100) obtained from FLAPW calculation [25].

and Jennings et al. [116] used Eq. (5) to describe the potential for $z>z_{im}$. For $z<z_{im}$ they utilized a model that is very different from Eqs. (3) and (4). Their model potential parameters were fitted to reproduce the FLAPW potential behaviour in the region close to the surface where the LDA gives an accurate description of the potential and the charge density distribution. Nevertheless, despite a different form of our potential and the potential of Refs. [116,131] and completely different physical quantities taken to fit the parameters of the models, we have very good agreement with z_{im} values calculated in Refs. [116,131]. The value of $z_{im}=2.18$ a.u. has been obtained by Smith et al. [131] by fitting the JJJ model potential [132] to the first and second image state energies within the two-band model [29]. From Table 7, it follows that a good agreement is also observed with the value of z_{im} found by Weinert et al. [30], who used another approximation for the description of a potential in the solid–vacuum interface region, and with the results of Refs. [9,31] where a simplified form of the crystal potential was used.

The Cu(111) surface represents another kind of the image potential states. On this surface the energy gap is located below the vacuum level (upper edge of the gap is 0.7 eV below E_V) and the first image state is at the top of this gap — just below the upper edge of the gap. All other image states degenerate with the bulk states. Such a position of the first image state influences its properties. In particular, the penetration of the $n=1$ state on this surface is greater than that on Cu(100) (see Tables 7 and 8). It leads to a shorter lifetime of the $n=1$ state on Cu(111) [16,17,23,57]. At the same time, owing to a resonance character of the second image state its lifetime is shorter than that of the $n=1$ state lifetime [16]. In Table 8 we present some experimental and theoretical data

Table 8
The Cu(111) surface (designations and units correspond to those in Table 1)

Characteristics	Experiment	Theory	Model potential
E_{edge}^{lower} ($L_{2'}$)	-0.90 ± 0.2[a]	-0.93[b]; -0.89[c]	-0.89
E_{edge}^{upper} (L_1)	–	3.7[b]; 4.25[c,d]	4.25
E_0	-0.39[e,f,g]	-0.5[h]; -0.59[i]; -0.46[j]	-0.39
E_1	-0.83[k]; -0.82[l]; -0.84[m]	-0.76[j]; -0.81[n]; -0.80[o]	-0.82
E_2^*	-0.25[l]; -0.26[m]	-0.20[n]; -0.22[o]	-0.22
E_3^*	-0.093[p]	–	-0.096 ± 0.003
E_4^*	-0.053[p]	–	-0.054 ± 0.003
p_1	–	79.0[q]	22.30
ϕ	4.94[q]	5.1[h]; 5.0[i]	4.94
z_{im}	–	2.14[o]; 2.35[r]; 2.27[s]	2.11

[a] Ref. [127].
[b] Ref. [74].
[c] Present LAPW calculation.
[d] Ref. [133].
[e] Ref [134].
[f] Ref. [135].
[g] Ref. [136].
[h] Ref. [137].
[i] Ref. [138].
[j] Ref. [31].
[k] Ref. [139].
[l] Ref. [16].
[m] Ref. [140].
[n] Ref. [46].
[o] Ref. [30].
[p] This value is obtained from the conventional Eq. (1), where $a=\sqrt{0.85/E_1}-1$. E_1 is the experimental or first-principles calculation energy value of the $n=1$ image state.
[q] Ref. [14].
[r] Ref. [116].
[s] Ref. [131].

characterizing the electronic structure of Cu(111). Comparing the calculated binding energy of the $n=2$ state with available experimental [16,140] and theoretical [30,46] results one can conclude that good agreement is observed with these data. The binding energies of higher image states obtained by direct calculation of the one-dimensional model potential Schrödinger equation agree well with those found from Eq. (1).

As in the case of Cu(100), our value of z_{im} for Cu(111) agrees very well with the results of other calculations [30,116,131]. Comparison of the calculated image plane positions for Cu(100) and Cu(111) with reference to the surface atomic layer shows that one can use $z_{im} \approx 2.2$ a.u. for both these surfaces. With reference to the geometrical edge this value is $z^{g}_{im} = 0.23$ a.u. for Cu(111) and $z^{g}_{im} = 0.49$ a.u. for Cu(100).

3.7. Ag(100) and Ag(111)

In Table 9 we show some experimental and theoretical data characterizing the electronic structure of Ag(100). To determine the model potential parameters A_1 and A_{10} we have used the IPE measured position of the lower edge of the energy gap [10] and the upper edge position obtained from our LAPW bulk calculation. The parameters A_2 and β are found by reproducing the experimental resonance surface state binding energy $E_0 = 1.3$ eV [10] and the first image state binding energy $E_1 = -0.53$ eV obtained with the use of 2PPE [126]. Comparing our results for the binding energies E_2 and E_3 with available experimental [14,126] and theoretical [14,30,43] results one can see good agreement with those data.

Our penetration values p_1 and p_2, compared with those estimated from the FLAPW evaluation [43], show a qualitative agreement with the first-principles calculation results. From Table 7 it follows that the p_n values of the image states on Ag(100) are very similar to those on Cu(100). One can also see from Table 9 that for Ag(100) fair agreement is observed between the image plane positions obtained from different methods. Our value $z_{im} = 2.06$ a.u. agrees acceptably well with that found by Ortuño and Echenique [31] and Smith et al. [131]. Worse agreement is observed with the z_{im} values calculated by Weinert et al. [30] and Aers and Inglesfield [142]. Weinert et al. [30] used a wave function matching technique that closely connects the image plane position with the image states binding energies. For $E_1 = -0.62$ eV they obtained $z_{im} = 2.64$ a.u. At the same time, a qualitative analysis of the problem [30,31, 39,40,131] shows that upon decreasing z_{im} the image state energy also decreases. Therefore, the use of the 2PPE measured value $E_1 = -0.53$ eV instead of $E_1 = -0.62$ eV should give a smaller value z_{im}. A graphical solution of the problem for this energy (see fig. 2 of Ref. [30] illustrating the problem for the Cu(100) surface) gives $z_{im} \approx 2.25$ a.u. We assume that the dependence of z_{im} on the image state energy is the same for Ag(100) because of the very close similarity of the

Table 9
The Ag(100) surface (designations and units correspond to those in Table 1)

Characteristics	Experiment	Theory	Model potential
E^{lower}_{edge} ($X_{4'}$)	1.6[a]	1.5[b]; 1.9[c]	1.6
E^{upper}_{edge} (X_1)	–	6.64[b]; 6.6[c]	6.64
E^{*}_{0}	1.3[a]	1.22[d]; 0.58[e]; 0.4[f]	1.3
E_1	−0.53[a,g]; −0.5[h]	−0.62[d]; −0.55[e]; −0.53[f]	−0.53
E_2	−0.16[g]	−0.19[d]; −0.17[e]	−0.17
E_3	−0.075[i]	−0.080[i]	−0.081
E_4	−0.047[j]	–	−0.048
p_1	–	<8.0[e]; 4.3[i]	5.24
p_2	–	<4.0[e]	0.98
p_3	–	–	0.33
p_4	–	–	0.15
ϕ	4.43[g,i]	4.53[e]; 4.95[k]; 4.4[l]	4.43
z_{im}	–	2.64[d]; 1.73[f]; 2.9[k]; 1.75[m]	2.06

[a] Ref. [10].
[b] Present LAPW calculation.
[c] Ref. [74].
[d] Ref. [30].
[e] Ref. [43].
[f] Ref. [31].
[g] Ref. [126].
[h] Ref. [141].
[i] Ref. [14].
[j] This value is obtained from the conventional Eq. (1), where $a = \sqrt{0.85/E_1} - 1$. E_1 is the experimental or first-principles calculation energy value of the $n=1$ image state.
[k] Ref. [142].
[l] Ref. [143].
[m] Ref. [131].

Table 10
The Ag(111) surface (designations and units correspond to those in Table 1)

Characteristics	Experiment	Theory	Model potential
E_{edge}^{lower} ($L_{2'}$)	–	-0.4[a,b]; -0.5[c]	-0.4
E_{edge}^{upper} (L_1)	–	3.6[a]; 3.9[b]	3.9
E_0	-0.065[d]	$+0.04$[e]; -0.16[f]	-0.065
E_1	-0.7[g]; -0.6[h]; -0.77[i,j]	-0.77[e]; -0.78[f]	-0.77
E_2^*	-0.23 ± 0.03[j]	-0.22[e]	-0.22 ± 0.01
E_3^*	-0.10 ± 0.03[j]	–	-0.095 ± 0.003
E_4^*	-0.052[k]	–	-0.053 ± 0.003
p_1	–	25.0[l]	23.4
ϕ	4.56[l]; 4.74[m]	4.67[n]	4.56
z_{im}	–	2.43[e]; 2.12[f]; 2.07[o]	2.22

[a] Ref. [74].
[b] Present LAPW calculation.
[c] Ref. [80].
[d] Ref. [135]
[e] Ref [30].
[f] Ref. [31].
[g] Ref. [144].
[h] Ref. [8].
[i] Ref. [81].
[j] Ref. [126].
[k] This value is obtained from the conventional Eq. (1), where $a=\sqrt{0.85/E_1}-1$. E_1 is the experimental or first-principles calculation energy value of the $n=1$ image state.
[l] Ref. [14].
[m] Ref. [145].
[n] Ref. [143].
[o] Ref. [131].

electronic structures of these surfaces for $E>E_F$. The value $z_{im}\approx2.25$ a.u. is in good agreement with ours despite the very different behaviour of the potential [30] in the metal–vacuum interface.

Qualitatively, the electronic structure of Ag(111) is similar to that of Cu(111), but, in contrast to Cu(111), no experimental information on the position of the energy gap edges is available. So, to fit the parameters A_1 and A_{10} our LAPW bulk calculation results are used (see Table 10). To determine the parameters A_2 and β we utilize the surface state energy $E_0=-0.065$ eV [135] and 2PPE value $E_1=-0.77$ eV [126] found experimentally at low temperature. The model potential calculation results are shown in Table 10 and it that excellent agreement is observed between the calculated and 2PPE measured binding energies for the $n=2, 3$ states. The value of z_{im} agrees well with the results obtained by Smith et al. [131], Ortuño and Echenique [31], and Weinert et al. [30].

3.8. Au(100) and Au(111)

It is well known that the stable crystal structure of Au(100) exhibits a (5×20) reconstruction [146]. The crystal structure (1×1) typical for the FCC(100) surfaces can be stabilized by impurities or defects [147,148]. The unoccupied surface electronic structure of Au(100) was studied with the use of IPE spectroscopy [10,42,44,129] for both these crystal structures. On both of these surfaces the first image state has been found, whereas the resonance surface state has been observed only on the metastable (1×1) surface. The difference between E_1 values measured on the (5×20) and (1×1) surfaces does not exceed 0.1 eV. We have used the experimental values $E_0=1.5$ eV and $E_1=-0.63$ eV to determine the parameters A_2 and β. To fit the parameters A_1 and A_{10} the IPE-measured position of the lower edge of the energy gap [10] and the calculated value [149] of the upper edge were utilized. The calculated binding energies of the $n=2, 3, 4$ image states, together with other results, are presented in Table 11. A comparison of the evaluated penetration values of p_n with those of Cu(100) and Ag(100) shows that a larger fraction of the image states wave functions penetrates into the bulk in the case of Au(100) than in the case of Cu(100) and Ag(100). Therefore, according to the penetration argument [52–54] one can expect a shorter lifetime of the image states on Au(100) than on the (100) surfaces of Cu and Ag. As for the image plane position, our $z_{im}=1.62$ a.u. value is in excellent agreement with $z_{im}=1.68$ a.u. evaluated by Smith et al. [131] by fitting the JJJ model potential to the first and second image state energies within the two-band gap model [29]. Both of these positions are inside the crystal, in contrast to $z_{im}=2.41$ a.u. obtained with the use of the JJJ model potential that was fitted to the FLAPW potential averaged in the x, y plane in the surface region [116,131].

The main difference between the Au(111) and Cu(111) [or Ag(111)] surfaces is that on Cu(111)

Table 11
The Au(100) surface (designations and units correspond to those in Table 1)

Characteristics	Experiment	Theory	Model potential
E_{edge}^{lower} ($X_{4'}$)	1.6[a]	1.4[b]; 1.5[c]	1.6
E_{edge}^{upper} (X_1)	–	5.8[c]	5.8
E_0^*	1.5[a]	1.45[b]	1.51 ± 0.01
E_1	-0.62[a]; -0.63[b,d]	-0.69[b]	-0.64
E_2	-0.183[e]	–	-0.188
E_3	-0.085[e]	–	-0.088
E_4	-0.049[e]	–	-0.051
p_1	–	–	7.00
p_2	–	–	1.48
p_3	–	–	0.52
p_4	–	–	0.24
ϕ	5.47[f]	4.53[b]; 6.16[g]	5.47
z_{im}	–	1.68[h]; 2.41[h]	1.62

[a] Ref. [10].
[b] Ref. [42].
[c] Ref. [149].
[d] Ref. [129].
[e] This value is obtained from the conventional Eq. (1), where $a=\sqrt{0.85/E_1}-1$. E_1 is the experimental or first-principles calculation energy value of the $n=1$ image state.
[f] Ref. [145].
[g] Ref. [79].
[h] Ref. [131].

Table 12
The Au(111) surface (designations and units correspond to those in Table 1)

Characteristics	Experiment	Theory	Model potential
E_{edge}^{upper} ($L_{2'}$)	-1.0[a]	-1.0[b]	-1.0
E_{edge}^{lower} (L_1)	3.6[a]	3.6[b]	3.6
E_0	-0.50[a]; -0.35[c]; -0.47[d]; -0.41[e]	-0.38[a]	-0.47
E_1^*	-0.6[a]; -0.42[f]; -0.8[g]	-0.85[a]; -0.87[h]; -0.68[i]	-0.80 ±0.01
E_2^*	-0.206[j]	-0.21[h]; -0.19[i]	-0.21 ±0.01
E_3^*	-0.093[j]	-0.09[h]	-0.095 ±0.002
E_4^*	-0.052[j]	–	-0.054 ±0.002
ϕ	5.55[g,h]; 5.31[k]	6.01[l]	5.55
z_{im}	–	2.18[m]	2.14

[a] Ref. [150].
[b] Ref. [153].
[c] Ref. [154].
[d] Ref. [135].
[e] Ref [152].
[f] Ref. [81].
[g] Ref. [151].
[h] Ref. [14].
[i] Ref. [46].
[j] This value is obtained from the conventional Eq. (1), where $a=\sqrt{0.85/E_1}-1$. E_1 is the experimental or first-principles calculation energy value of the $n=1$ image state.
[k] Ref. [145].
[l] Ref. [79].
[m] Ref. [131].

the first image state is located at the top of the energy gap, whereas on Au(111) this state degenerates with bulk states [14,81,150,151]. The upper edge of the energy gap on Au(111) is ~2 eV below E_V and 2PPE experiment gives $E_1=-0.80$ eV [14,151]. In contrast to the simple metal surfaces on Au(111), both IPE [81,150] and 2PPE [151] experiments show a clear feature in the spectra corresponding to the $n=1$ image state. A clear peak generated by the first image state is also obtained in the model potential calculation. The parameters A_1 and A_{10} of the model potential have been adjusted to reproduce experimentally found positions of the energy gap edges [150]. The parameters A_2 and β describe the occupied surface state energy [152] and $E_1=-0.80$ eV [14,151] at $\bar{\Gamma}$. The model potential calculation results for Au(111) are listed in Table 12. It follows from Table 12 that our E_2 value agrees well with other model calculations [14,46]. Close agreement is observed between the one-dimensional model potential Schrödinger equation eigenvalues and solutions of Eq. (1) for $n=2, 3, 4$.

Again, as occurs for the Au(100) surface, our value of $z_{im}=2.14$ a.u. for Au(111) is very close to $z_{im}=2.18$ a.u. obtained by Smith et al. [131]. It seems surprising, at first sight, because these authors used in their calculation a value of $E_1=-0.6$ eV. In fact, they determined z_{im} by using the surface state energy $E_0=-0.41$ eV only, and this is the reason for the good agreement with our z_{im}. The use of $E_1=-0.6$ eV only gives an anomalously small value of $z_{im}\approx1.1$ a.u.

A graphical solution of the problem for $E_1=-0.8$ eV (see fig. 2 of Ref. [131]) gives $z_{im}\approx1.9$ a.u., which is in much better agreement with our z_{im} value.

3.9. Pd(111) and Pd(100)

The surface electronic structure of Pd(111) is quite different from that of Cu(111), Ag(111),

and Au(111). In particular, on Pd(111) the lower edge of the energy gap is above the Fermi level, and all image states are located just above the middle of the gap. From this point of view the Pd(111) surface is more similar to the (100) surface than to that of the (111) of Cu, Ag, and Au. In contrast to Cu(111), the surface state on Pd(111) is unoccupied at the $\bar{\Gamma}$ point. The energies E_0 and E_1 have been measured with the use of both IPE and 2PPE spectroscopies [82,155,156]. For the surface state these measurements gave a practically identical result of $E_0 \approx 1.3$ eV. As for the first image state they gave quite different values of E_1. To fit the parameters A_2 and β we have used the 2PPE-measured value of $E_1 = 0.55$ eV [155]. To determine A_1 and A_{10} we utilized the positions of the lower and upper edges of the energy gap obtained from our LAPW bulk calculation. Table 13 lists some model potential calculation results and other theoretical and experimental data and, as can be seen, our E_2 value agrees well with experimental [155] and calculation [82,155] results. For higher image states an excellent agreement is obtained between the one-dimensional model potential Schrödinger equation eigenvalues and energies of Eq. (1). On the other hand, the image states energies evaluated by Lenac et al. [32] seem to be too large.

A comparison of our z_{im} value with those obtained from other calculations shows extremely good agreement with the z_{im} value obtained by Hulbert et al. [82] and with z_{im} found in the self-energy calculation of the seven- to nine-layer films of Pd(111) [45], and large disagreement with the one found by Lenac et al. [32]. The slight discrepancy with the calculation [131] may be due to the value $E_1 = -0.65$ eV used in Ref. [131]. The use of a value of $E_1 = -0.55$ eV should increase z_{im}, thus leading to a better agreement with our result.

In contrast to the Pd(111) surface, for Pd(100) there are no available experimental data on unoccupied electron states. The only HREELS measurement gave for two image states $E_1 = -0.95$ eV and $E_2 = -0.19$ eV [161]. It seems that the first image state energy is too large for a state located inside the energy gap. This result may be influenced significantly by the low resolution of the HREELS technique [161]. In order to determine the parameters A_1 and A_{10}, in describing the energy gap we have utilized our LAPW bulk calculation data (see Table 14). The evaluated positions $E_{X_4'} = 3.5$ eV and $E_{X_1} = 10.6$ eV, of the lower and upper edges respectively, of the energy gap are in good agreement with other calculations [74,157]. To obtain the parameters A_2 and β we use the resonance surface state energy $E_0 = 1.9$ eV found in our LAPW film calculation. Because of the absence of any IP or 2PPE measurement of the binding

Table 13
The Pd(111) surface (designations and units correspond to those in Table 1)

Characteristics	Experiment	Theory	Model potential
E_{edge}^{lower} ($L_{2'}$)	–	0.95[a]; 1.0[b]; 0.7[c]; 1.3[d]	1.0
E_{edge}^{upper} (L_1)	7.7 ± 0.3[e]	7.3[a]; 7.6[b]; 7.2[c]	7.6
E_0	1.3[f]; 1.26[g]	1.28[f]; 1.17[g]; 2[h]; 0.54[i]; 1.74[i]; 1.1[j]; 0.9[k]	1.3
E_1	−0.50[f]; −0.55[g]; −0.65[l]; −0.75[m]	−0.52[f]; −0.58[g]; −0.72[i]; −0.69[k]	−0.55
E_2	−0.15[g]; −0.25[m]	−0.17[f]; −0.18[g]; −0.22[i]	−0.17
E_3	−0.081[n]	−0.08[g]; −0.096[i]	−0.082
E_4	−0.047[n]	–	−0.048
p_1	–	4.5[o]	4.60
p_2	–	–	0.86
p_3	–	–	0.29
p_4	–	–	0.13
ϕ	5.44[g]; 5.55[l]	5.46[g]; 6.18[k]; 5.53[p]	5.44
z_{im}	–	2.25[f]; 3.97[i]; 2.48[k]; 1.99[q]	2.29

[a] Ref. [157].
[b] Present LAPW calculation.
[c] Ref. [74].
[d] Ref. [80].
[e] Ref. [158].
[f] Ref. [82].
[g] Ref. [155].
[h] Ref. [159].
[i] Ref. [32].
[j] Ref. [160].
[k] Ref. [45].
[l] Ref. [156].
[m] Ref. [161].
[n] This value is obtained from the conventional Eq. (1), where $a = \sqrt{0.85/E_1} - 1$. E_1 is the experimental or first-principles calculation energy value of the $n = 1$ image state.
[o] Ref. [14].
[p] Ref. [143].
[q] Ref. [131].

Table 14
The Pd(100) surface (designations and units correspond to those in Table 1)

Characteristics	Experiment	Theory	Model potential
E_{edge}^{lower} (X_4')	–	3.3[a]; 3.5[b]; 3.6[c]	3.5
E_{edge}^{upper} (X_1)	–	10.5[a]; 10.6[b]; 10.54[c]	10.6
E_0^*	1.0 ± 0.2[d]	1.9[b]	1.9
E_1	-0.9 ± 0.2[d]; -0.95[e]	-0.53[f]; -0.60[g]	-0.5
E_2	-0.19[e]; -0.160[h]	–	-0.163
E_3	-0.078[h]	–	-0.079
E_4	-0.046[h]	–	-0.047
p_1	–	–	3.54
p_2	–	–	0.66
p_3	–	–	0.22
p_4	–	–	0.10
ϕ	5.3[i]; 5.8[j]; 5.22[k]; 5.55[k]	5.6[b]; 6.11[g]; 5.0[i]; 5.25[l]; 5.3[m]; 5.8[n]; 5.96[o]	5.6
z_{im}	–	2.39[f]; 2.31[g]	2.29

[a] Ref. [74].
[b] Present LAPW calculation.
[c] Ref. [157].
[d] Ref. [162].
[e] Ref. [161].
[f] Ref. [131].
[g] Ref. [45].
[h] This value is obtained from the conventional Eq. (1), where $a=\sqrt{0.85/E_1}-1$. E_1 is the experimental or first-principles calculation energy value of the $n=1$ image state.
[i] Ref. [163].
[j] Ref. [164].
[k] Ref. [165].
[l] Ref. [166].
[m] Ref. [143].
[n] Ref. [167].
[o] Ref. [79].

energy of the first image state the image plane position of Pd(111) $z_{im}=2.29$ a.u. is taken as a second value to fit A_2 and β. This choice of z_{im} for Pd(100) seems to be reasonable. In particular, Smith et al. [131] evaluated z_{im} for Pd(100) and Pd(110) using the FLAPW planar average potential. They found a very slight dependence (0.06 a.u.) of z_{im} on the surface. This means one can expect a change in z_{im} between the closed-packed (100) and (111) surfaces of the same order as the change between the closed-packed (100) face and relatively open (110) face. One can note that in the recent self-energy calculation [45] $z_{im}=2.31$ a.u. has been obtained for Pd(100). The present evaluation gives $E_1=-0.5$ eV, which agrees well with the corresponding value of -0.53 eV predicted by Smith et al. [131] within their model and with $E_1=-0.60$ eV found in the self-consistent calculation by Heinrichsmeier et al. [45]. The calculated penetration values of image states on Pd(100) are smaller than those on Pd(111); therefore, one can expect a longer lifetime for image states on Pd(100). On the other hand, the phase space available for decay of an electron from image state to final (unoccupied) states is significantly larger for Pd(100) than for Pd(111). Therefore, the role of final states may be dominant on the Pd(100) surface, leading to a shorter lifetime value of image states on this surface.

4. General discussion and conclusion

The present calculations demonstrate in accordance with other evaluations [28,36,39,41] that the binding energy of the first image state on simple metal surfaces lies in an energy interval from ~-1.0 eV to ~-0.7 eV. Other calculations [33,34,37,38] performed for the aluminium surfaces (111) and (100) give $E_1\simeq-0.5$ eV in agreement with available experimental data [48–50] for Al(111). Because of very weak character of the feature in the spectra, corresponding to the first image state on Al(111), and the low resolution of the IPE spectroscopy technique, it is very difficult to expect that these experiments can provide compelling evidence that the binding energy of the $n=1$ state is about of -0.5 eV. The Be(0001) surface could be a very good object to observe a resonance image state. In contrast to the case of Al(111), the calculated density of states for Be(0001) has a clear peak corresponding to the first image state. The measurement of the $n=1$ state on Be(0001) could give additional information about the binding energy value of this state on Al(111), since it is difficult to expect a qualitatively different behaviour of image states on these close-packed surfaces. The main distinction between these two surfaces with respect to image states is the different electron reflectivity, produced by the bulk band structure. The Au(111) surface can provide another indirect argument in favour of the binding energy to be about -0.8 eV. On Au(111) the first image state is the typical resonance one, which is easily seen from the calculated

density of states and from 2PPE measurement [151].

Our model potential describes one of the key quantities used in the calculations of the image states lifetime, namely, wave functions of image states, in excellent agreement with those obtained from the first principles calculations. The evaluation of the lifetime of image states for the Cu(100) and Cu(111) surfaces [57] shows good agreement with recent TR2PPE measurements [16,17,23] and emphasizes the crucial need of a precise description of the image state wave function. Moreover, this model potential describes accurately the wave function of the $n=0$ s–p_z surface state at the $\bar{\Gamma}$ point. The self-energy calculation [168] of the linewidth of this occupied state at $\bar{\Gamma}$ leads to excellent agreement with recent very high-resolution angle-resolved photoemission measurements for Cu(111) [169,170] and with scanning tunneling spectroscopy (STS) experiments for Ag(111) [171]. The calculated inelastic linewidth for Cu(111) has been found to be of 25 meV, whereas the measurements give 21 ± 5 meV [170] and 30 meV [169]. For the surface state linewidth on Ag(111) the calculation gives 3.2 meV, and the STS-measured value is 4.8 ± 1.2 meV [171].

Our model potential calculations give the new set of image plane position values for simple and noble metal surfaces. In general, these values are smaller than those obtained from evaluations of the linear response to a test charge for simple metal surfaces. At the same time the GW self-energy calculations place z_{im} closer to the surface atomic layer than our calculations do. In the case of noble metals our z_{im} values agree well with those obtained by Smith et al. [131] within a phase-shift model combined with the two-band approximation and with those found by Jennings et al. [116] from the surface charge density profile. Excellent agreement is observed with z_{im} obtained from the electronic self-energy calculations for Pd(111) and Pd(100) [45].

Acknowledgements

The authors are grateful to U. Höfer, Th. Fauster, W. Plummer, E. Zaremba, Yu.M. Koroteev, A. Rivacoba, and A.G. Lipnitskii for useful discussions. This project has been supported by the Ministerio de Educación y Cultura, Spain, the Departamento de Educación del Gobierno Vasco, and Iberdrola S.A.

Appendix A

Table 15 gives the model potential parameters A_{10}, A_1, A_2, β and interlayer spacing value a_s. All other model potential parameters are obtained from these using the requirement of continuity of the potential and its first derivative everywhere in space.

Table 15

Surface	a_s (a.u.)	A_{10} (eV)	A_1 (eV)	A_2 (eV)	β
Li(110)	4.667	−7.768	2.99	2.2425	2.0760
Na(110)	5.733	−6.100	0.67	0.8710	2.8934
Be(0001)	3.387	−18.750	6.20	4.1354	4.2630
Mg(0001)	4.923	−10.550	0.70	1.2600	4.7223
Al(100)	3.80	−15.690	1.68	2.0160	5.1258
Al(111)	4.388	−15.700	0.30	1.9500	5.7276
Cu(100)	3.415	−11.480	6.10	3.7820	2.5390
Cu(111)	3.94	−11.895	5.14	4.3279	2.9416
Ag(100)	3.86	−9.300	5.04	3.8808	2.4222
Ag(111)	4.43	−9.640	4.30	3.8442	2.5649
Au(100)	3.853	−10.810	4.20	6.0690	3.3626
Au(111)	4.45	−11.030	4.60	4.8576	2.8239
Pd(111)	4.25	−8.570	6.60	4.6728	1.9071
Pd(100)	3.68	−8.480	7.10	5.0481	1.8460

References

[1] I.E. Tamm, Z. Phys. 76 (1932) 849.
[2] W. Shockley, Phys. Rev. 56 (1939) 317.
[3] P.M. Echenique, J.B. Pendry, J. Phys. C 11 (1978) 2065.
[4] P.M. Echenique, J.B. Pendry, Prog. Surf. Sci. 32 (1990) 111.
[5] F.J. Himpsel, Comments Condens. Matter Phys. 12 (1986) 199.
[6] N.V. Smith, Rep. Prog. Phys. 51 (1988) 1227.
[7] R.M. Osgood Jr., X. Wang, Solid State Phys. 51 (1997) 1.
[8] A. Goldmann, V. Dose, G. Borstel, Phys. Rev. B 32 (1985) 1971.
[9] G. Borstel, G. Thörner, Surf. Sci. Rep. 8 (1988) 1.
[10] F.J. Himpsel, J.E. Ortega, Phys. Rev. B 46 (1992) 9719.
[11] M. Donath, Surf. Sci. Rep. 20 (1994) 251.
[12] K. Giesen, F. Hage, F.J. Himpsel, H.J. Riess, W. Steinmann, Phys. Rev. Lett. 55 (1985) 300.
[13] W. Merry, R.E. Jordan, D.E. Padowitz, C.B. Harris, Surf. Sci. 295 (1993) 393.
[14] Th. Fauster, W. Steinmann, in: P. Halevi (Ed.), Electromagnetic Waves: Recent Development in Research vol. 2, Elsevier, Amsterdam, 1995, p. 350.
[15] R.W. Schoenlein, J.G. Fujimoto, G.L. Eesley, T.W. Capehart, Phys. Rev. Lett. 61 (1988) 2596.
[16] M. Wolf, E. Knoesel, T. Hertel, Phys. Rev. B 54 (1996) R5295.
[17] U. Höfer, I.L. Shumay, Ch. Reuß, U. Thomann, W. Wallauer, Th. Fauster, Science 277 (1997) 1480.
[18] R.L. Lingle Jr., N.H. Ge, R.E. Jordan, J.D. McNeil, C.B. Harris, J. Chem. Phys. 205 (1996) 191.
[19] F.J. Himpsel, Phys. Rev. B 43 (1991) 13 394.
[20] S. Bode, K. Starke, P. Rech, G. Kaindl, Phys. Rev. Lett. 72 (1994) 1072.
[21] E. Passek, M. Donath, K. Ertl, V. Dose, Phys. Rev. Lett. 75 (1995) 2746.
[22] R.W. Schoenlein, J.G. Fujimoto, G.L. Eesley, T.W. Capehart, Phys. Rev. B 43 (1991) 4688.
[23] I.L. Shumay, U. Höfer, Ch. Reuß, U. Thomann, W. Wallauer, Th. Fauster, Phys. Rev. B 58 (1998) 13 974.
[24] J.D. McNeil, R.L. Lingle Jr,, N.H. Ge, C.M. Wong, R.E. Jordan, C.B. Harris, Phys. Rev. Lett. 79 (1997) 4645.
[25] S.L. Hulbert, P.D. Johnson, M. Weinert, R.F. Garrett, Phys. Rev. B 33 (1986) 760.
[26] S. Papadia, M. Persson, L.-A. Salmi, Phys. Rev. B 41 (1990) 10 237.
[27] M. Nekovee, S. Crampin, J.E. Inglesfield, Phys. Rev. Lett. 70 (1993) 3099.
[28] T. Fondén, S. Papadia, M. Persson, J. Phys. Condens. Matter 7 (1995) 2697.
[29] N.V. Smith, Phys. Rev. B 32 (1985) 3549.
[30] M. Weinert, S.L. Hulbert, P.D. Johnson, Phys. Rev. Lett. 55 (1985) 2055.
[31] M. Ortuño, P.M. Echenique, Phys. Rev. B 34 (1986) 5199.
[32] Z. Lenac, M. Šunjić, H. Conrad, M.E. Kordesch, Phys. Rev. B 36 (1987) 9500.
[33] S.Å. Lindgren, L. Walldén, Phys. Rev. B 40 (1989) 11 546.
[34] L. Jurczyszyn, M. Stęślicka, Surf. Sci. 266 (1992) 141.
[35] Th. Fauster, Appl. Phys. A 59 (1994) 639.
[36] L. Jurczyszyn, M. Stęślicka, Surf. Sci. 376 (1997) L424.
[37] M. Radny, Surf. Sci. 231 (1990) 43.
[38] A.G. Eguiluz, M. Heinrichsmeier, A. Fleszar, W. Hanke, Phys. Rev. Lett. 68 (1992) 1359.
[39] M. Nekovee, J.E. Inglesfield, Europhys. Lett. 19 (1992) 535.
[40] V.M. Silkin, E.V. Chulkov, Phys. Solid State 36 (1994) 404, Rus. Fiz. Tverd. Tela 36 (1994) 736.
[41] F. Finocchi, C.M. Bertoni, S. Ossicini, Vacuum 41 (1990) 535.
[42] F. Ciccacci, S. De Rossi, A. Taglia, S. Crampin, J. Phys. Condens. Matter 6 (1994) 7227.
[43] Z. Li, S. Gao, Phys. Rev. B 50 (1994) 15349.
[44] S. De Rossi, F. Ciccacci, S. Crampin, Phys. Rev. Lett. 77 (1996) 908.
[45] M. Heinrichsmeier, A. Fleszar, W. Hanke, A. Eguiluz, Phys. Rev. B 57 (1998) 14 974.
[46] L. Jurczyszyn, Surf. Sci. 259 (1991) 65.
[47] M. Nekovee, J. Inglesfield, Prog. Surf. Sci. 50 (1995) 149.
[48] D. Heskett, K.-H. Frank, E.E. Koch, H.-J. Freund, Phys. Rev. B 36 (1987) 1276.
[49] S. Yang, R.A. Bartynski, G.P. Kochanski, S. Papadia, T. Fondén, M. Persson, Phys. Rev. Lett. 70 (1993) 849.
[50] V. Bulovič, B. Quiniou, R.M. Osgood Jr., J. Vac. Sci. Technol. A: 12 (1994) 2201.
[51] E.V. Chulkov, V.M. Silkin, P.M. Echenique, Surf. Sci. 391 (1997) L1217.
[52] P.M. Echenique, F. Flores, F. Sols, Phys. Rev. Lett. 55 (1985) 2348.
[53] P. de Andres, P.M. Echenique, F. Flores, Phys. Rev. B 35 (1987) 4529.
[54] P. de Andres, P.M. Echenique, F. Flores, Phys. Rev. B 39 (1989) 10 356.
[55] J. Deisz, A. Fleszar, M. Heinrichsmeier, A. Eguiluz, unpublished results.
[56] S. Gao, B.I. Lundqvist, Prog. Theor. Phys. 106 (suppl. N) (1991) 405.
[57] E.V. Chulkov, I. Sarría, V.M. Silkin, J.M. Pitarke, P.M. Echenique, Phys. Rev. Lett. 80 (1998) 4947.
[58] J. Osma, I. Sarría, E.V. Chulkov, J.M. Pitarke, P.M. Echenique, Phys. Rev. B 59 (1999) 10 591.
[59] E.V. Chulkov, J. Osma, I. Sarría, V.M. Silkin, J.M. Pitarke, Surf. Sci. (1999) in press.
[60] G.B. Bachelet, D.R. Hamann, M. Schlüter, Phys. Rev. B 26 (1982) 4199.
[61] V.M. Silkin, E.V. Chulkov, I.Yu. Sklyadneva, V.E. Panin, Izv. Vuzov. Fiz. 9 (1984) 56.
[62] E.V. Chulkov, V.M. Silkin, E.N. Shyrikalov, Fiz. Met. Metall. 64 (1987) 213.
[63] W. Kohn, L.J. Sham, Phys. Rev. 140 (1965) A1133.
[64] L. Hedin, B.I. Lundqvist, J. Phys. C 4 (1971) 2064.
[65] N.D. Lang, W. Kohn, Phys. Rev. B 7 (1973) 3541.
[66] M.W. Finnis, R. Kaschner, C. Kruse, J. Furthmüller, M. Scheffler, J. Phys. Condens. Matter 7 (1995) 2001.

[67] S. Ossicini, C.M. Bertoni, P. Gies, Europhys. Lett. 1 (1986) 661.
[68] P.A. Serena, J.M. Soler, N. Garcia, Phys. Rev. B 37 (1988) 8701.
[69] I.D. White, R.W. Godby, M.M. Rieger, R.J. Needs, Phys. Rev. Lett. 80 (1998) 4265.
[70] J.A. Appelbaum, D.R. Hamann, Phys. Rev. B 6 (1972) 1122.
[71] V.M. Silkin, E.V. Chulkov, P.M. Echenique, Phys. Rev. B 60 (1999) Sept. 15.
[72] H. Krakauer, M. Posternak, A.J. Freeman, Phys. Rev. B 19 (1979) 1706.
[73] D.R. Hamann, Phys. Rev. Lett. 42 (1979) 662.
[74] D.A. Papaconstantopoulos, The Band Structure of Elemental Solids, Plenum, New York, 1986.
[75] J.E. Northrup, M.S. Hybertsen, S.G. Louie, Phys. Rev. B 39 (1989) 8198.
[76] A.P. Ovchinnikov, B.M. Tsarev, Fiz. Tverd. Tela (Leningrad) 9 (1967) 3512, Sov. Phys. Solid State 9 (1968) 2766.
[77] K. Kokko, P.T. Salo, R. Laihia, K. Mansikka, Surf. Sci. 384 (1996) 168.
[78] N.D. Lang, W. Kohn, Phys. Rev. B 3 (1971) 1215.
[79] H.L. Skriver, N.M. Rosengaard, Phys. Rev. B 46 (1992) 7157.
[80] V.L. Moruzzi, J.F. Janak, A.R. Williams, Calculated Electronic Properties of Metals, Pergamon, New York, 1978.
[81] D. Straub, F.J. Himpsel, Phys. Rev. B 33 (1986) 2256.
[82] S.L. Hulbert, P.D. Johnson, M. Weinert, Phys. Rev. B 34 (1986) 3670.
[83] S. Andersson, J.B. Pendry, P.M. Echenique, Surf. Sci. 65 (1977) 539.
[84] R.L. Gerlach, T.N. Rhodin, Surf. Sci. 19 (1970) 403.
[85] T. Rodach, K.P. Bohnen, K.M. Ho, Surf. Sci. 209 (1989) 481.
[86] N.W. Ashcroft, J. Phys. Chem. 1 (1968) 232.
[87] U.O. Karlsson, S.A. Flodström, R. Engelhardt, W. Gädeke, E.E. Koch, Solid State Commun. 49 (1984) 711.
[88] R.A. Bartynski, E. Jepsen, T. Gustafsson, E.W. Plummer, Phys. Rev. B 32 (1985) 1921.
[89] E.V. Chulkov, V.M. Silkin, E.N. Shirykalov, Surf. Sci. 188 (1987) 287.
[90] P.J. Feibelman, Phys. Rev. B 46 (1992) 2532.
[91] N.A.W. Holzwarth, Y. Zeng, Phys. Rev. B 51 (1995) 13 653.
[92] P.A. Bruhwiller, G.M. Watson, E.W. Plummer, H.J. Sagner, K.H. Frank, Europhys. Lett. 11 (1990) 573.
[93] G.M. Watson, P.A. Bruhwiller, H.J. Sagner, K.H. Frank, E.W. Plummer, Phys. Rev. B 50 (1994) 17 678.
[94] E. Jensen, R.A. Bartynski, T. Gustafsson, E.W. Plummer, M.Y. Chou, M.L. Cohen, G.B. Hoflund, Phys. Rev. B 30 (1984) 5500.
[95] A.K. Green, E. Bauer, Surf. Sci. 74 (1978) L676.
[96] R.A. Bartynski, R.H. Gaylord, T. Gustafsson, E.W. Plummer, Phys. Rev. B 33 (1986) 3644.
[97] E.W. Plummer, Surf. Sci. 152–153 (1985) 162.
[98] U.O. Karlsson, G.V. Hansson, P.E.S. Persson, S.A. Flodström, Phys. Rev. B 26 (1982) 1852.
[99] E.V. Chulkov, V.M. Silkin, Solid State Commun. 58 (1986) 273.
[100] H.J. Levinson, F. Greuter, E.W. Plummer, Phys. Rev. B 27 (1983) 727.
[101] G.V. Hansson, S.A. Flodström, Phys. Rev. B 18 (1978) 1562.
[102] G.V. Hansson, S.A. Flodström, Phys. Rev. B 19 (1979) 3329.
[103] E. Caruthers, L. Kleinman, G.P. Alldredge, Phys. Rev. B 8 (1973) 4570.
[104] H. Krakauer, M. Posternak, A.J. Freeman, D.D. Koelling, Phys. Rev. B 23 (1981) 3859.
[105] M. Seel, Phys. Rev. B 28 (1983) 778.
[106] G. Wachutka, Phys. Rev. B 34 (1986) 8512.
[107] J.E. Inglesfield, G.A. Benesh, Surf. Sci. 200 (1988) 135.
[108] E.V. Chulkov, V.M. Silkin, Surf. Sci. 215 (1989) 385.
[109] M. Heinrichsmeier, A. Fleszar, A.G. Eguiluz, Surf. Sci. 285 (1993) 129.
[110] S.P. Singhal, J. Callaway, Phys. Rev. B 16 (1977) 1744.
[111] P.O. Gartland, B.J. Slagsvold, Solid State Commun. 25 (1978) 489.
[112] J.K. Grepstad, P.O. Gartland, B.J. Slagsvold, Surf. Sci. 57 (1976) 348.
[113] R.M. Eastman, C.H.B. Mee, J. Phys. F 3 (1973) 1738.
[114] R. Stumpf, M. Scheffler, Phys. Rev. B 53 (1996) 4958.
[115] K.P. Bohnen, K.M. Ho, Surf. Sci. 207 (1988) 105.
[116] P.J. Jennings, R.O. Jones, M. Weinert, Phys. Rev. B 37 (1988) 6113.
[117] J.E. Inglesfield, Vacuum 41 (1990) 543.
[118] S.D. Kevan, N.G. Stoffel, N.V. Smith, Phys. Rev. B 31 (1985) 1788.
[119] E. Caruthers, L. Kleinman, G.P. Alldredge, Phys. Rev. B 9 (1974) 3330.
[120] K. Mednick, L. Kleinman, Phys. Rev. B 22 (1980) 5768.
[121] F. Schreier, F. Rebentrost, J. Phys. C 20 (1987) 2609.
[122] S.C. Lam, R.J. Needs, J. Phys. Condens. Matter 5 (1993) 2101.
[123] A. Euceda, D.M. Bylander, L. Kleinman, K. Mednick, Phys. Rev. B 27 (1983) 659.
[124] D.S. Wang, A.J. Freeman, H. Krakauer, Phys. Rev. B 26 (1982) 1340.
[125] D.P. Woodruff, S.L. Hulbert, P.D. Johnson, N.V. Smith, Phys. Rev. B 31 (1985) 4046.
[126] K. Giesen, F. Hage, F.J. Himpsel, H.J. Riess, W. Steinmann, Phys. Rev. B 35 (1987) 971.
[127] J.A. Knapp, F.J. Himpsel, D.E. Eastman, Phys. Rev. B 19 (1979) 4952.
[128] G. Thörner, G. Borstel, V. Dose, J. Rogozik, Surf. Sci. 157 (1985) L379.
[129] D. Straub, F.J. Himpsel, Phys. Rev. Lett. 52 (1984) 1922.
[130] V. Dose, W. Altmann, A. Goldmann, U. Kolac, J. Rogozik, Phys. Rev. Lett. 52 (1984) 1919.
[131] N.V. Smith, C.T. Chen, M. Weinert, Phys. Rev. B 40 (1989) 7565.

[132] R.O. Jones, P.J. Jennings, O. Jepsen, Phys. Rev. B 29 (1984) 6474.
[133] J.F. Janak, A.R. Williams, V.L. Moruzzi, Phys. Rev. B 11 (1975) 1522.
[134] S.D. Kevan, Phys. Rev. Lett. 50 (1983) 526.
[135] R. Paniago, R. Matzdorf, G. Meister, A. Goldmann, Surf. Sci. 336 (1995) 113.
[136] P.O. Gartland, B.J. Slagsvold, Phys. Rev. B 12 (1975) 4047.
[137] J.A. Appelbaum, D.R. Hamann, Solid State Commun. 27 (1978) 881.
[138] A. Euceda, D.M. Bylander, L. Kleinman, Phys. Rev. B 28 (1983) 528.
[139] K. Giesen, F. Hage, F.J. Himpsel, H.J. Riess, W. Steinmann, Phys. Rev. B 33 (1986) 5241.
[140] G.D. Kubiak, Surf. Sci. 201 (1988) L475.
[141] B. Reihl, K.H. Frank, R.R. Schlittler, Phys. Rev. B 30 (1984) 7328.
[142] G.C. Aers, J.E. Inglesfield, Surf. Sci. 217 (1989) 367.
[143] M. Methfessel, D. Hennig, M. Scheffler, Phys. Rev. B 46 (1992) 4816.
[144] S.L. Hulbert, P.D. Johnson, N.G. Stoffel, N.V. Smith, Phys. Rev. B 32 (1985) 3451.
[145] H.B. Michelson, J. Appl. Phys. 48 (1977) 4729.
[146] D.G. Fedak, N.A. Gjostein, Surf. Sci. 8 (1967) 77.
[147] J.F. Wendelken, D.M. Zehner, Surf. Sci. 71 (1978) 178.
[148] P. Heimann, J. Hermanson, H. Miosga, H. Neddermeyer, Phys. Rev. Lett. 43 (1979) 1757.
[149] N.E. Christensen, B.O. Seraphin, Phys. Rev. B 4 (1971) 3321.
[150] D.P. Woodruff, W.A. Royer, N.V. Smith, Phys. Rev. B 34 (1986) 764.
[151] C. Reuß, W. Wallauer, Th. Fauster, Surf. Rev. Lett. 3 (1994) 1547.
[152] S.D. Kevan, R.H. Gaylord, Phys. Rev. B 36 (1987) 5809.
[153] A.B. Chen, B. Segall, Solid State Commun. 18 (1976) 149.
[154] R. Courths, H. Wern, U. Hau, B. Cord, V. Bachelier, S. Hüfner, J. Phys. F 14 (1984) 1559.
[155] R. Fischer, S. Schuppler, N. Fischer, Th. Fauster, W. Steinmann, Phys. Rev. Lett. 70 (1993) 654.
[156] G.D. Kubiak, J. Vac. Sci. Technol. A: 5 (1987) 731.
[157] N.E. Christensen, Phys. Rev. B 14 (1976) 3446.
[158] F.J. Himpsel, D.E. Eastman, Phys. Rev. B 18 (1978) 5236.
[159] S.G. Louie, Phys. Rev. Lett. 40 (1978) 1525.
[160] W. Dong, G. Krese, J. Furthmüller, J. Hafner, Phys. Rev. B 54 (21) (1996) 57.
[161] H. Conrad, M.E. Cordesch, W. Stenzel, M. Sunjić, B. Trninic-Radja, Surf. Sci. 178 (1986) 578.
[162] S.C. Wu, D.M. Poirier, M.B. Jost, J.H. Weaver, Phys. Rev. B 45 (1992) 8709.
[163] J.G. Gay, J.R. Smith, F.J. Arlinghaus, T.W. Capehart, Phys. Rev. B 23 (1981) 1559.
[164] J. Rogozik, J. Küppers, V. Dose, Surf. Sci. 148 (1984) L653.
[165] J. Hölzl, F.K. Schulte, in: Work Function of MetalsSolid Surface Physics vol. 85 Springer, Heidelberg, 1979.
[166] D. Tománek, Z. Sun, S.G. Louie, Phys. Rev. B 43 (1991) 4699.
[167] A. Wachter, K.P. Bohnen, K.M. Ho, Surf. Sci. 346 (1996) 127.
[168] E.V. Chulkov, V.M. Silkin, P.M. Echenique, in preparation.
[169] B.A. McDougall, T. Balasubramanian, E. Jensen, Phys. Rev. B 51 (1995) 13 891.
[170] F. Theilmann, R. Matzdorf, G. Meister, A. Goldmann, Phys. Rev. B 56 (1997) 3632.
[171] J. Li, W.-D. Schneider, R. Berndt, O.R. Bryant, S. Crampin, Phys. Rev. Lett. 81 (1998) 4464.